

Six-jet production at lepton colliders¹

S. Moretti

*Rutherford Appleton Laboratory,
Chilton, Didcot, Oxon OX11 0QX, UK.*

Abstract

We study electron-positron annihilations into six jets at the parton level in perturbative Quantum Chromo-Dynamics (QCD), via the elementary processes $e^+e^- \rightarrow q\bar{q}gggg$, $e^+e^- \rightarrow q\bar{q}q'\bar{q}'gg$ and $e^+e^- \rightarrow q\bar{q}q'\bar{q}'q''\bar{q}''$, for massive quarks q, q' and q'' and massless gluons g . Several numerical results of phenomenological relevance are given, at three different collider energies and for a representative selection of jet clustering algorithms. We also present helicity amplitudes and colour factors needed for the tree-level calculation.

PACS: 12.38.-t, 12.38.Bx, 13.87.-a, 13.65.+i

Keywords: perturbative QCD, LO computations, jets, lepton colliders.

¹E-mail: moretti@v2.rl.ac.uk.

1 Introduction and motivation

1.1 Multi-jet rates

As the centre-of-mass (CM) energy of modern accelerators grows, the number of final state partons that can be accommodated in the available phase space becomes larger. Many of these will be quarks and gluons, as QCD forces are the strongest among the fundamental interactions. In electron-positron annihilations, coloured partons can be produced via an initial splitting of a γ or Z current into quark-antiquark pairs, followed by no hard radiation at all or by (multiple) gluon bremsstrahlung, with the vector particles eventually yielding further quark-antiquark pairs or other gluons, as schematically recalled in Fig. 1.

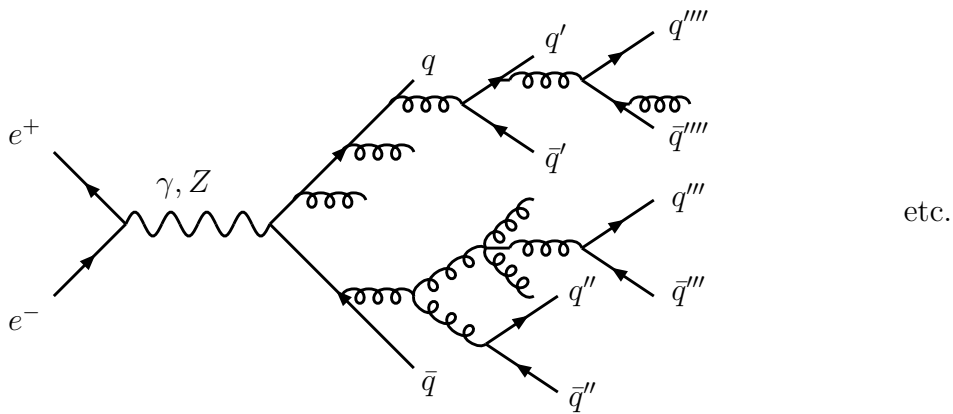


Figure 1: Schematic description of multi-parton production in e^+e^- annihilations.

Clearly, as this so-called *parton shower* or *cascade* evolves in time, the amount of energy exchanged among the various partons diminishes, so that the process will eventually enter a non-perturbative regime. At such low energy scales (roughly, of the order of 1 GeV), one is unable to describe quantitatively the above process in terms of a series expansion in powers of the strong coupling constant α_s using Feynman diagram techniques, since α_s becomes significantly large and the series cannot be resummed reliably. Note that 1 GeV is also the scale at which the partons are conventionally assumed to hadronise, that is, to convert themselves into the observed hadrons through the formation of colourless bound states (see Ref. [1] for an up-to-date review of hadronisation mechanisms), which in turn make up the jets observed in the experimental apparatus.

This fact clearly illustrates an intrinsic limitation of the perturbative approach. A further, more practical, restraint that one has to face is due to our scarce ability for calculating multi-particle amplitudes using standard perturbative techniques. In fact, with the number

of final states particles increasing, the complexity of the expressions of the fundamental scattering amplitudes and the large number of terms involved (arising from the combinatorics of the diagrams) that one has to master become in the end an obstacle difficult to overcome, in spite of the help of modern computers. For example, if one limits oneself in Fig. 1 to the case of gluon radiation only (that is to $q\bar{q} + ng$ final states), one has the following impressive escalation of numbers of Feynman diagrams involved (considering the γ and Z propagators together): 1 for $n = 0$, 2 for $n = 1$, 8 for $n = 2$, 50 for $n = 3$, 428 for $n = 4$, 4670 for $n = 5$, etc².

An even higher degree of complications is encountered if one goes beyond the leading order (LO) and tries to incorporate loop corrections in the calculation. In fact, it should be recalled that the actual number of jets produced in electron-positron annihilations is defined according to a phenomenological *jet clustering* algorithm, in which jets are constructed out of primary objects (hereafter, labelled by i, j etc.), the latter being hadrons or calorimeter cells in the real experimental case and partons in the theoretical calculation. The term *exclusive* means that each primary object is assigned to a unique jet and each final state has a unique jet multiplicity, for a given value of the jet *resolution parameter* y_{cut} . Algorithms of this type are generically based on a binary clustering, wherein the number of objects is reduced one at a time by combining the two nearest (in some sense) ones. The joining procedure is stopped by testing against some criterion (the parameter y_{cut}), and the final clusters are called jets (we will treat some of these algorithms in greater detail later on, in Subsect. 2.2).

From the point of view of perturbative calculations, it is evident that the n -jet rate will then be constituted not only of the fraction of n -parton events in which all partons are resolved, but also by the $(n + m)$ -parton contributions (with $m \geq 1$) in which m partons remain unresolved. Now, in the $(n + m)$ -parton $\rightarrow n$ -jet transitions, two partons can well be combined in singular configurations. This can happen when one has either two collinear partons within or one soft parton outside the ‘jet cones’. Both these contributions are (in general, positively) divergent. Thanks to the Bloch-Nordsieck [4] and Kinoshita-Lee-Nauenberg [5] theorems (see also Ref. [6]), these collinear and soft singularities are cancelled at the same order in α_s by the divergent contributions (generally, negative) provided by the virtual loop graphs. If one recombination has occurred then one-loop diagrams must be computed, when two mergings have taken place two-loop graphs are needed, and so on. As a matter of fact, the computation of loop diagrams is even more demanding than that of tree-level ones (both using trace [7] and helicity [8] techniques). Not surprisingly then, the number of *exact* calculations of $e^+e^- \rightarrow n$ -parton matrix elements (ME) available in the

²Under these circumstances, the use of spinor techniques based on the helicity decomposition of the Feynman amplitudes becomes mandatory, in order to simplify the calculation to a certain extent (for a good introduction to helicity methods and complete references, see [2] and [3]).

literature is rather limited.

As for the tree-level, till a few years ago only up to five-parton final states were computed, via the elementary scatterings: $e^+e^- \rightarrow q\bar{q}ggg$ and $e^+e^- \rightarrow q\bar{q}q'\bar{q}'g$. This calculation was tackled in Ref. [9]. The case of four partons via $e^+e^- \rightarrow q\bar{q}gg$ and $e^+e^- \rightarrow q\bar{q}q'\bar{q}'$ has been known since long time [10]. The case of three partons (i.e., $e^+e^- \rightarrow q\bar{q}g$) was very trivial [1] and the lowest-order case of two (i.e., $e^+e^- \rightarrow q\bar{q}$) is in fact a textbook example [11]. Only recently, the task of computing six-parton cross sections (via $e^+e^- \rightarrow q\bar{q}gggg$, $e^+e^- \rightarrow q\bar{q}q'\bar{q}'gg$ and $e^+e^- \rightarrow q\bar{q}q'\bar{q}'q''\bar{q}''$) has been accomplished, in Ref. [12], where numerical results for the massless case were presented. It is the main purpose of the present paper to present new phenomenological analyses of six-jet production at lepton colliders as well as to give the analytical expressions corresponding to those six-parton processes, further extending the calculations of Ref. [12] to the case of quarks with generic mass. Notice that the retention of finite values of $m_{q,q',q''}$ in the amplitudes turns out to be a serious complication in many instances, because of the unavoidable proliferation of terms and/or the slowness of execution of the numerical routines that it generates. As a matter of fact, depending on the CM energy, the actual flavour of the quark being produced and also the region in phase space under study, in many cases the effect of the masses can safely be ignored³.

As for loop and radiative diagrams, the highest-order corrections calculated to date in $e^+e^- \rightarrow n$ -jet annihilations are the next-to-leading order (NLO) ones to the four-jet rate, that is, terms proportional to α_s^3 [13, 14], in the massless approximation. The α_s^2 ones date back to Ref. [10] for the massless case while the massive one has been completed very recently [15]. In fact, considerable simplifications can be attained also at loop level when the quark mass is neglected. Two- and higher-order-loop corrections are not yet known.

But let us review the theoretical progress in evaluating $e^+e^- \rightarrow n$ -parton rates and its interplay with the experiment. This will also eventually help us to motivate the need of the availability of the calculations carried out in Ref. [12] and in this paper.

The history of calculations of multi-jet production in e^+e^- scatterings [16]–[28] began at the times when jets were first observed at PEP and PETRA. At those energies the Z contribution was small and could safely be ignored [10], [16]–[19], (see also [21, 23]). Mass effects were already taken into account in some instances. However, apart from the simplest cases [16, 17], only the formulae for massless fermions were compact enough to be published [10, 18, 22]. With the advent of LEP and the advances in spinor techniques these results were improved in various ways. In particular, in [25] the complete triply differential cross section

³So was the case before the LEP era for the more complicated contribution of the intermediate Z (and its interference with the photon) in the primary e^+e^- annihilation, provided the energy at which the latter takes place is well below the mass of the former (at PEP and PETRA, for example).

for $e^+e^- \rightarrow q\bar{q}g$ for massive quarks with both intermediate photon and Z was presented. In Ref. [26] the decay $Z \rightarrow 4f$ (with $f = q$ or ℓ : i.e., quark or lepton) was studied and from the expression given there it is possible to reconstruct the full amplitude for $e^+e^- \rightarrow q\bar{q}q'\bar{q}'$. Very simple formulae for $e^+e^- \rightarrow q\bar{q}gg$, $q\bar{q}q'\bar{q}'$ were given in Ref. [27] for massless quarks. The tree-level amplitudes for three-, four- and five-parton events including all mass effects and both the γ and Z contributions were given in analytic form in Refs. [29, 30]. Finally, one-loop three-parton and tree-level four-parton terms have been combined and incorporated in Monte Carlo simulation programs [31, 32, 33], as has been done for the one-loop four-parton and tree-level five-parton amplitudes [34, 35, 36], for massless quarks in both cases, whereas the massive contributions to the α_s^2 three-jet rates with massive partons will soon be.

A further point should be noted. On the one hand, at small values of the resolution parameter y_{cut} , the fixed-order perturbative calculations of n -jet rates become unreliable because of the presence of large logarithms of the form $\ln(y_{\text{cut}})$ (in other words, because of the growing of the $(n+m)$ -jet contributions, with $m \geq 1$). On the other hand, the exact higher order calculations can be technically unavailable. Under these circumstances, the resummation to all α_s orders in perturbation theory of terms of the form $\mathcal{O}(\alpha_s^n \ln^m(1/y))$, e.g., with $m = l$ and $m = l - 1$ (to leading and next-to-leading accuracy, with n and m depending on the jet observable), can improve substantially the reliability of the theoretical predictions, as was shown to be the case for the two- and tree-jet rates [37]–[41]. Recall, however, that such a resummation is only possible within the framework of certain jet clustering schemes, such as the Durham and Cambridge ones (see Subsect. 2.2), for which the jet fractions show the usual Sudakov exponentiation of multiple soft-gluon emission.

The availability of three-, four- and five-parton matrix elements (tree- and loop-level and supplemented with the mentioned logarithms resummed) has been of crucial importance in studying the underlying structure of QCD. Throughout the years and at different colliders (PEP, PETRA, LEP, SLC), several tests have been performed. The strong coupling constant α_s has been determined from jet rates and from shape variables [42] and both the flavour independence and the running with \sqrt{s} have been verified (see, e.g., Ref. [43]). Three- [44] and four-jet [45] differential distributions have been long studied and their behaviour agrees with QCD predictions calculated to second and third order in α_s , respectively. The colour factors, which determine the gauge group responsible for strong interactions, have been measured [46, 47]. Models alternative to QCD have been ruled out and the coupling of the triple gluon vertex has been verified to be consistent with the QCD theory [48]. The latest QCD tests are currently being carried out at LEP2. In addition, at this energy, one of the key issues is to quantify to a high degree of accuracy the amount of background in multi-jet events from QCD to the W^+W^- hadronic decays, as the corresponding signal (though biased by systematic uncertainties due to relatively unknown Bose-Einstein [49]

and Colour Interconnection [50] effects) still represents to date the experimentally preferred decay channel, because of its somewhat higher statistics and because kinematic constraints can tighten the precision of M_{W^\pm} measurements [51, 52].

In the not too distant future (presumably not long after the year 2005), a new electron-positron machine will be operative, the Next Linear Collider (NLC), which is expected to run initially at an energy of 500 GeV, later increasing up to 2 TeV or so.

1.2 Six-jet rates

The phenomenology of six-jet events produced in electron-positron annihilations (shown schematically in Fig. 2) is not as all well known as that of smaller multiplicity jet rates, from both the experimental and theoretical point of view. This should not sound surprising, given the complications arising from, on the one hand, the poor event rate and large number of tracks, and, on the other hand, the mentioned complexity of the perturbative QCD calculations.

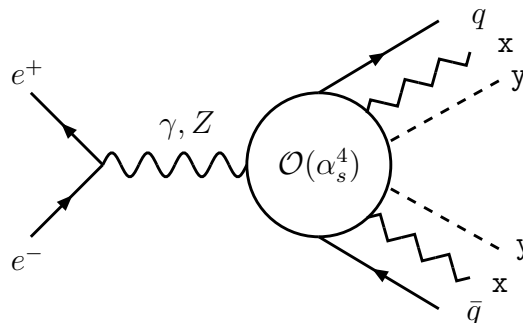


Figure 2: Schematic Feynman diagrams contributing in lowest order to $e^+e^- \rightarrow 6$ partons. The jagged and dashed lines and the labels x, y refer to either a quark or a gluon, see (1)–(3).

In our opinion, the time has now come to approach the calculation of $e^+e^- \rightarrow 6$ jet events. We are driven to this belief from the following considerations. LEP1 was the era of the Z -peak and of its two-jet (and several higher-order) decays. LEP2 is now the age of the W^+W^- -resonance and of its four-jet (and some higher-order) decays. As we will move into the NLC epoch, we will step into a long series of resonant processes, typically ending up with six-jet signatures. One can mention top physics for a start. As this is one of the main goals of the NLC, we should expect a lot of experimental studies concerned with $t\bar{t} \rightarrow b\bar{b}W^+W^- \rightarrow 6$ jet-events, since the W^\pm 's mainly decay hadronically into two jets. Then one should not forget the new generation of gauge boson resonances, such as W^+W^-Z and ZZZ , and their favourite six-jet decays. One could also add highly-virtual

photonic processes, like $\gamma W^+ W^-$, γZZ , $\gamma\gamma Z$ and $\gamma\gamma\gamma$ as well as those involving the Higgs particle, via $ZH \rightarrow ZW^+ W^-$, $ZH \rightarrow ZZZ$ and $ZH \rightarrow ZHH$, provided this is light enough to be produced at those energy regimes.

A collection of dedicated articles illustrating the phenomenology of top-antitop and three-boson production at NLC can be found in Ref. [53]. It is beyond the scope of this paper to recall the salient features of those studies and the interplay of the mentioned resonant events with the six-jet background produced via QCD. Instead, what we would like to emphasise here, is that one should be ready with all the appropriate phenomenological instruments to challenge the new kind of multi-jet experimental studies that will have to be carried out at the new generation of e^+e^- machines.

As for the theoretical progress in this respect, studies of $e^+e^- \rightarrow 6$ -fermion electroweak processes are under way. A brief account of approaches and methods can be found in Ref. [54]. These kinds of reactions have already been calculated and analysed for the case involving up to four quarks in the final state [55] (and other similar studies are in preparation [56]), while in Ref. [57] the concern was for Higgs processes with two quarks produced. One should probably expect the upgrade of the codes used for those studies to the case of six-quark production via electroweak interactions quite soon. However, a large fraction of the six-jet cross section comes from QCD interactions involving gluon propagators, gluon emissions and quark-gluon couplings. The case of six-jet production from W^+W^- decays was considered in Ref. [58].

In the present paper, the main focus will be on the $\mathcal{O}(\alpha_s^4)$ QCD processes at tree-level:

$$e^+e^- \rightarrow q\bar{q}gggg, \quad (1)$$

$$e^+e^- \rightarrow q\bar{q}q'\bar{q}'gg \quad (2)$$

$$e^+e^- \rightarrow q\bar{q}q'\bar{q}'q''\bar{q}'', \quad (3)$$

where q, q' and q'' represent any possible flavours of quarks (massless and/or massive) and g is the QCD gauge boson.

As a by-product of our analysis, we will study the case of electromagnetic (EM) radiation. Since the QED emission of photons off quark lines is dynamically similar to that of gluons (apart from the different strength of the coupling and the colour factor associated with it), we will modify our MEs with external gluons (1)–(2) appropriately, so as to allow for the case of multiple hard photon emission from the final state (Final State Radiation, FSR), in $e^+e^- \rightarrow q\bar{q}ggg\gamma$, $e^+e^- \rightarrow q\bar{q}gg\gamma\gamma$, $e^+e^- \rightarrow q\bar{q}g\gamma\gamma\gamma$, $e^+e^- \rightarrow q\bar{q}\gamma\gamma\gamma\gamma$ (via two-quark) and $e^+e^- \rightarrow q\bar{q}q'\bar{q}'g\gamma$, $e^+e^- \rightarrow q\bar{q}q'\bar{q}'\gamma\gamma$ (via four-quark) events. In order to calculate the photoproduction cross sections, we further supplement the FSR diagrams with those in which photon emission takes place from the initial state (Initial State Radiation, ISR) along with

those in which photons are radiated from both the incoming and outgoing fermions. Notice that hard photons produced by electrons and positrons can also be included by means of a convolution of the non-radiative diagrams with the so-called Electron Structure Functions (ESF) [59]. Such implementation allows one to include the exact photon corrections to the e^+e^- annihilation subprocess resummed up to the third order [60] in the EM coupling constant α_{em} in the infrared limit (in particular, they embody both soft/collinear and virtual photon emission). We have not exploited here this approach, as we have used our tree-level diagrams. In doing so, however, additional cuts are necessary in order to screen our results from the collinear singularities due to the infrared emission from the initial state. We have required $p_T^\gamma > 5$ GeV and $|\cos\theta_\gamma| < 0.85$. Such cuts are similar to the photon selection criteria adopted by the LEP Collaborations.

We will apply our results to the case of LEP1, LEP2 and, particularly, NLC energies. A short description of the computational techniques adopted will be given in Sect. 2. Results are in Sect. 3. A brief summary is given in Sect. 4. The explicit helicity amplitude formulae are in Appendix I, whereas the colour factors are presented in Appendix II.

2 Matrix Elements

In order to master the large number of Feynman diagrams (of the order of several hundred) entering in processes (1)–(3) at tree-level, we have used spinor methods [3]. In fact, if one adopts the technique of deriving the expression of the squared amplitude $|A|^2 = |\sum_k a_k|^2$ by using the textbook method of the traces (a_k being the amplitude associated to diagram k), one results in a prohibitive number of terms to be evaluated. Typically, if n is the number of diagrams, then $\frac{n(n+1)}{2}$ traces have to be computed. Recalling the numbers of Sect. 1, the task is clearly prohibitive for six-parton events. The calculation becomes simpler if one uses so-called ‘helicity amplitude’ (or ‘spinor’) techniques. In such an approach, given a set of helicities assigned to the external particles, one computes the contribution of every single diagram k as a complex number a_k , sums over all k ’s and takes the modulus squared. This way, in the above example, one only needs to compute n (complex) terms. To obtain unpolarised cross sections one simply sums the modulus squared for the various helicity combinations. Thus, a further advantage is intrinsic to the spinor method, that one can naturally compute also polarised MEs (e.g., for the SLC and NLC), without the need of inserting into the expression of the amplitudes the helicity projection operators [61].

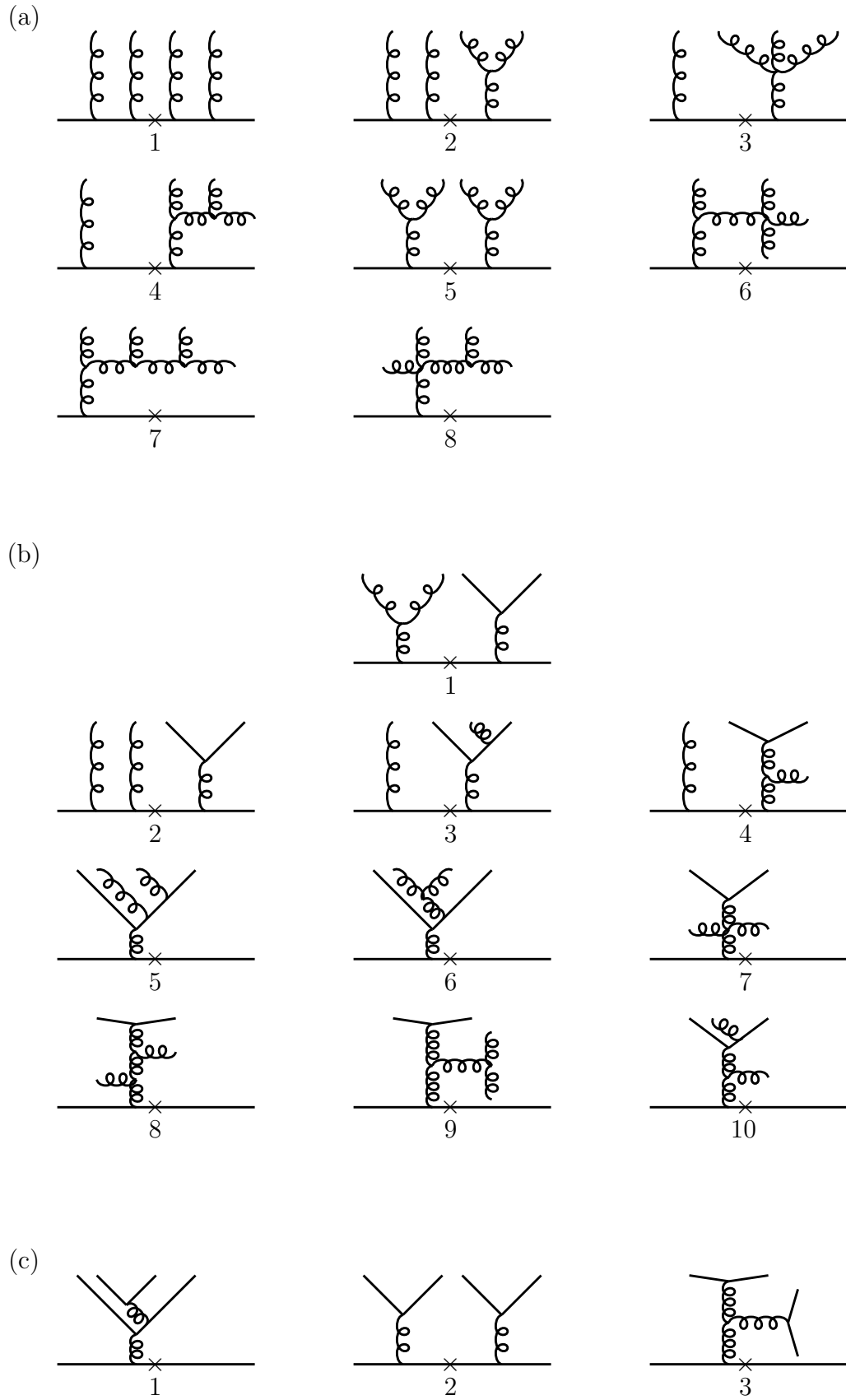


Figure 3: Tree-level Feynman topologies contributing to: (a) $e^+e^- \rightarrow q\bar{q}gggg$, (b) $e^+e^- \rightarrow q\bar{q}q'\bar{q}'gg$ and (c) $e^+e^- \rightarrow q\bar{q}q'\bar{q}'q''\bar{q}''$. The symbol \times refers to the insertion of the $e^+e^- \rightarrow \gamma, Z$ current. Permutations are not shown.

2.1 The spinor methods

The use of helicity amplitude techniques in high energy physics dates back to Refs. [62, 63]. Since then, many different approaches have been developed [64]–[75] and a review of the vast literature on this subject is beyond the intentions of this paper. For this, we remind the reader of Ref. [2]. Of those available in literature, we employed here *two* methods. We have done so in order to be able to check adequately the correctness of our calculations, as usual tests of gauge invariance might fail to reveal possible *bugs* in the numerical codes. Note that the two methods can be used both with massless and massive particles.

The first one is based on the formalism of Ref. [72] and exploits the `HELAS` subroutines [76]. It is the same already employed to produce the numerical results presented in [12]. Here, one adopts a specific representation for the Dirac matrices. It is then possible to obtain explicit expressions for the spinors, for the matrices at the vertices and for the fermion propagators, and thus the components of the polarisation vectors of the gauge bosons can be written directly in terms of their four-momenta. The complex number corresponding to a given diagram is obtained by multiplying these matrices. Therefore, one most conveniently programs the amplitudes directly as deduced from the Feynman rules and no manipulations on these need be performed. Masses in this case turn out to be an entry in a propagator matrix. It would be possible to consider some algebraic simplifications of the formulae, e.g., by separating the two independent chirality components of the *massless* spinors and cancelling by hand the terms proportional to the quark masses. However, the method of Ref. [72] is particularly well suited for numerical calculations and such algebraic treatment would not significantly improve the speed of the programs. Therefore, we have not exploited here any chiral decomposition in case of massless spinors. Under these circumstances, the analytical expressions in the formalism of Ref. [72] would simply be a rewriting of the Feynman rules with the mentioned matrices expressed explicitly in terms of the external momenta and helicities, an exercise that we do not perform here.

A second approach was based on the method developed in Refs. [69, 73, 74, 77]. Since we will express the helicity amplitudes in this formalism, we will devote some space to its technicalities. (This is also helpful in order to introduce a notation that will be used in the Appendices and to render the formulae appearing there more transparent to the reader.)

In this method, all spinors for any physical momentum are defined in terms of a basic spinor of an auxiliary light-like momentum. By decomposing the internal momenta in terms of the external ones, using Dirac algebra and rewriting the polarisation of external vectors by means of a spinor current, all amplitudes can eventually be reduced to an algebraic combination of spinors products $\bar{u}(p_i)u(p_j)$ (with i, j, \dots labelling the external particles).

$\lambda_1 \lambda_3$	$X(p_1, \lambda_1; p_2, p_3, \lambda_3; c_R, c_L)$
++	$(\mu_1 \eta_2 + \mu_2 \eta_1)(c_R \mu_2 \eta_3 + c_L \mu_3 \eta_2) + c_R S(+, p_1, p_2) S(-, p_2, p_3)$
+-	$c_L(\mu_1 \eta_2 + \mu_2 \eta_1) S(+, p_2, p_3) + c_L(c_L \mu_2 \eta_3 + c_R \mu_3 \eta_2) S(+, p_1, p_2)$

Table 1: The X functions for the two independent helicity combinations in terms of the functions S , η and μ defined in the text. The remaining X functions can be obtained by flipping the sign of the helicities and exchanging $+$ with $-$ in the S functions and R with L in the chiral coefficients.

$\lambda_1 \lambda_2 \lambda_3 \lambda_4$	$Z(p_1, \lambda_1; p_2, \lambda_2; p_3, \lambda_3; p_4, \lambda_4; c_R, c_L; c'_R, c'_L)$
++++	$-2[S(+, p_3, p_1) S(-, p_4, p_2) c'_R c_R - \mu_1 \mu_2 \eta_3 \eta_4 c'_R c_L - \eta_1 \eta_2 \mu_3 \mu_4 c'_L c_R]$
+++ -	$-2\eta_2 c_R [S(+, p_4, p_1) \mu_3 c'_L - S(+, p_3, p_1) \mu_4 c'_R]$
++ - +	$-2\eta_1 c_R [S(-, p_2, p_3) \mu_4 c'_L - S(-, p_2, p_4) \mu_3 c'_R]$
+ - ++	$-2\eta_4 c'_R [S(+, p_3, p_1) \mu_2 c_R - S(+, p_3, p_2) \mu_1 c_L]$
++ --	$-2[S(+, p_1, p_4) S(-, p_2, p_3) c'_L c_R - \mu_1 \mu_2 \eta_3 \eta_4 c'_L c_L - \eta_1 \eta_2 \mu_3 \mu_4 c'_R c_R]$
+ - +-	0
+ - - +	$-2[\mu_1 \mu_4 \eta_2 \eta_3 c'_L c_L + \mu_2 \mu_3 \eta_1 \eta_4 c'_R c_R - \mu_2 \mu_4 \eta_1 \eta_3 c'_L c_R - \mu_1 \mu_3 \eta_2 \eta_4 c'_R c_L]$
+ - --	$-2\eta_3 c'_L [S(+, p_2, p_4) \mu_1 c_L - S(+, p_1, p_4) \mu_2 c_R]$

Table 2: The Z functions for all independent helicity combinations in terms of the functions S , η and μ defined in the text. The remaining Z functions can be obtained by flipping the sign of the helicities and exchanging $+$ with $-$ in the S functions and R with L in the chiral coefficients.

(i) *Spinors*. External fermions⁴ of mass m and momentum p^μ are described by spinors corresponding to states of definite helicity λ , $u(p, \lambda)$ ⁵, verifying the Dirac equations

$$\not{p} u(p, \lambda) = \pm m u(p, \lambda), \quad \bar{u}(p, \lambda) \not{p} = \pm m \bar{u}(p, \lambda), \quad (4)$$

and the spin sum relation

$$\sum_{\lambda=\pm} u(p, \lambda) \bar{u}(p, \lambda) = \not{p} \pm m, \quad (5)$$

where the sign $+$ ($-$) refers (here and in the following) to a particle(antiparticle). One can

⁴Unless stated otherwise, we shall use the term “fermion” and the symbol “ u ” for both particles and antiparticles.

⁵Here, $p(\lambda)$ represents a generic (anti)spinor four-momentum(helicity).

choose two arbitrary vectors k_0 and k_1 such that

$$k_0 \cdot k_0 = 0, \quad k_1 \cdot k_1 = -1, \quad k_0 \cdot k_1 = 0, \quad (6)$$

and express the spinors $u(p, \lambda)$ in terms of chiral ones $w(k_0, \lambda)$ as

$$u(p, \lambda) = w(p, \lambda) + \mu w(k_0, -\lambda), \quad (7)$$

where

$$w(p, \lambda) = \not{p} w(k_0, -\lambda) / \eta, \quad (8)$$

and

$$\mu = \pm \frac{m}{\eta}, \quad \eta = \sqrt{2|p \cdot k_0|}. \quad (9)$$

The spinors $w(k_0, \lambda)$ satisfy

$$w(k_0, \lambda) \bar{w}(k_0, \lambda) = \frac{1 + \lambda \gamma_5}{2} \not{k}_0, \quad (10)$$

and therefore

$$\sum_{\lambda=\pm} w(k_0, \lambda) \bar{w}(k_0, \lambda) = \not{k}_0. \quad (11)$$

The phase between chiral states is fixed by

$$w(k_0, \lambda) = \lambda \not{k}_1 w(k_0, -\lambda). \quad (12)$$

The freedom in choosing k_0 and k_1 provides a powerful tool for checking the correctness of any calculation. A convenient, though not unique choice, is the following: $k_0 = (1, 0, 0, -1)$ and $k_1 = (0, 1, 0, 0)$ [74]. In such a case the *massless* spinors in the two methods [69] and [72] coincide exactly, so that it is possible to compare in greater detail the two corresponding numerical codes. In particular, the results obtained with the two formalisms must agree for every single diagram and every polarisation of external particles.

(ii) *Polarisation vectors for massless gauge bosons*⁶. External spin 1 massless gauge bosons of momentum p^μ are described by polarisation vectors corresponding to states of definite helicity λ , $\varepsilon^\mu(p, \lambda)$, fulfilling the identities

$$\varepsilon(p, \lambda) \cdot p = 0, \quad \varepsilon(p, \lambda) \cdot \varepsilon(p, \lambda) = 0, \quad (13)$$

$$\varepsilon^\mu(p, -\lambda) = \varepsilon^{\mu*}(p, \lambda), \quad \varepsilon(p, \lambda) \cdot \varepsilon(p, -\lambda) = -1, \quad (14)$$

⁶Polarisation vectors for massive gauge bosons can be introduced on a similar footing, however, since we do not need them for our calculation, we refer the reader to the mentioned bibliography for this particular case.

and the spin sum relation (e.g., in the axial gauge)

$$\sum_{\lambda=\pm} \varepsilon^\mu(p, \lambda) \varepsilon^{\nu*}(p, \lambda) = -g^{\mu\nu} + \frac{q^\mu p^\nu + q^\nu p^\mu}{p \cdot q}, \quad (15)$$

where q^μ is any four-vector not proportional to p^μ . Any object $\varepsilon^\mu(p, \lambda)$ obeying the relations (14)–(15) makes an acceptable choice for the polarisation vectors. For instance

$$\varepsilon^\mu(p, \lambda) = N[\bar{u}(p, \lambda) \gamma^\mu u(q, \lambda)], \quad (16)$$

N being the normalisation factor

$$N = [4(q \cdot p)]^{-1/2}. \quad (17)$$

The existing freedom in choosing q^μ corresponds to fixing the gauge. The final results do not depend on the choice of q^μ .

(iii) *The S , X and Z functions.* Using the above definitions one can compute the functions

$$S(\lambda, p_1, p_2) = [\bar{u}(p_1, \lambda) u(p_2, -\lambda)], \quad (18)$$

$$X(p_1, \lambda_1; p_2; p_3, \lambda_3; c_R, c_L) = [\bar{u}(p_1, \lambda_1) \not{p}_2 \Gamma u(p_3, \lambda_3)], \quad (19)$$

and

$$\begin{aligned} Z(p_1, \lambda_1; p_2, \lambda_2; p_3, \lambda_3; p_4, \lambda_4; c_R, c_L; c'_R, c'_L) = \\ [\bar{u}(p_1, \lambda_1) \Gamma^\mu u(p_2, \lambda_2)] [\bar{u}(p_3, \lambda_3) \Gamma'_\mu u(p_4, \lambda_4)], \end{aligned} \quad (20)$$

where

$$\Gamma^{(\prime)\mu} = \gamma^\mu \Gamma^{(\prime)}, \quad (21)$$

and

$$\Gamma^{(\prime)} = c_R^{(\prime)} P_R + c_L^{(\prime)} P_L, \quad (22)$$

with

$$P_R = \frac{1 + \gamma_5}{2}, \quad P_L = \frac{1 - \gamma_5}{2}, \quad (23)$$

the chiral projectors.

By computing the resulting traces one easily finds ($\epsilon^{0123} = 1$ is the Levi-Civita tensor) [69, 73]

$$S(+, p_1, p_2) = 2 \frac{(p_1 \cdot k_0)(p_2 \cdot k_1) - (p_1 \cdot k_1)(p_2 \cdot k_0) + i \epsilon_{\mu\nu\rho\sigma} k_0^\mu k_1^\nu p_1^\rho p_2^\sigma}{\eta_1 \eta_2}, \quad (24)$$

for the S functions and the expressions listed in Tabs. 1 and 2 for the X and Z functions, respectively. For the S functions, one has $S(-, p_1, p_2) = S(+, p_2, p_1)^*$, while the remaining X and Z functions can be obtained as described in the captions of Tabs. 1–2.

The colour factors have been calculated with two different methods, as illustrated in Ref. [78] and by means of the techniques reported in Ref. [79]. Some possible expressions of both the amplitudes and the colour matrices will be given in the Appendices. The coded helicity amplitudes have been checked for gauge invariance and integrated using **VEGAS** [80], in both formalisms. The agreement at the (squared) amplitude level is always within 12 significant digits in **REAL*8** precision.

Although the actual number of Feynman diagrams needed to compute processes (1)–(3) is very large, only a much smaller portion of different topologies⁷ describe these. In fact, in the case of two-quark-four-gluon diagrams the topologies are those shown in Fig. 3(a), eight in total. For four-quark-two-gluons, Fig. 3(b), one has ten and for six-quarks, Fig. 3(c), three topologies. The same implementation of each of the topologies pictured in Fig. 3 can then be used several times by means of recursive permutations of the momenta of the external particles. Furthermore, each common ‘sub-topology’ to those in Fig. 3 is saved and then reused in the same numerical evaluation. The actual number of Feynman diagrams corresponding to the topologies in Fig. 3, including all possible permutations of momenta and counting as either one or three each diagram involving a four-gluon vertex (which carries in fact three different colour structures), is given in Tab. 3.

2.2 Jet clustering algorithms

As jet clustering algorithms we have adopted the Jade (J) [81], Durham (D) [82] and Cambridge (C) [83] schemes⁸. The first one uses the expression

$$y_{ij}^J = \frac{2E_i E_j (1 - \cos \theta_{ij})}{s}, \quad (25)$$

for the ‘jet measure’, whereas the other two are based on the same test variables

$$y_{ij}^{D,C} = \frac{2 \min(E_i^2, E_j^2) (1 - \cos \theta_{ij})}{s}, \quad (26)$$

but differ in the clustering procedure. In eqs. (25)–(26), E_i and E_j represent the energies of any pair of partons i and j , whereas θ_{ij} is their relative angle. A six-jet sample is selected by imposing the constraint $y_{ij} \geq y$ on all n possible parton combinations ij (with $n = 15$

⁷By ‘topology’ we mean a collection of Feynman diagrams which differ only in the permutations of gauge vectors along the fermion lines (neglecting their colour structure).

⁸In this Section as well as in the following ones, in order to simplify the notation, we shall use y to represent y_{cut} , the jet resolution parameter discussed in Sect. 1. In addition, we acknowledge here our abuse in referring to the various jet ‘finders’ both as algorithms and as schemes, since the last term was originally intended to identify the composition law of four-momenta when pairing two clusters. This is in fact a well admitted habit which we believe will not generate confusion in our discussion.

$e^+e^- \rightarrow q\bar{q}gggg$									
a1	a2	a3	a4	a5	a6	a7	a8		
120	144	24[72]	72	36	8[24]	12	12[36]		
Total 428[516]									
$e^+e^- \rightarrow q\bar{q}q'\bar{q}'gg \ (q \neq q')$									
b1	b2	b3	b4	b5	b6	b7	b8	b9	b10
12	48	48	24	24	8	4[12]	8	4	16
Total 196[204]									
$e^+e^- \rightarrow q\bar{q}q'\bar{q}'q''\bar{q}'' \ (q \neq q' \neq q'')$									
c1	c2	c3							
24	18	6							
Total 48									

Table 3: Number of Feynman diagrams corresponding to the topologies in Fig. 2. If two quark flavours are identical, numbers are multiplied by two, if three are, by six. In square brackets are the same numbers if the four-gluon diagrams are counted thrice, according to their three colour structures.

for the Jade and Durham and $5 \leq n \leq 15$ for the Cambridge algorithm). The $n = 15$ pairs of the J and D schemes are simply obtained by pairing all partons in the final state in all possible different combinations ij . The variable number $5 \leq n \leq 15$ for the C scheme is a consequence of the so-called ‘soft freezing’ step, which is described in [83], to which we refer the reader for further details.

2.3 Numerical parameters

We have adopted $M_Z = 91.17$ GeV, $\Gamma_Z = 2.516$ GeV, $\sin^2 \theta_W = 0.23$, $\alpha_{em} = 1/128$ and, unless otherwise stated, the two-loop expression for α_s , with $\Lambda_{\text{QCD}}^{n_f=4} = 0.298$ GeV. We have kept all quarks massless as a default, to speed up the numerical evaluation. Though, in several instances we have retained a finite value for the bottom mass, i.e., $m_b = 4.25$ GeV. Electron and positron have mass zero too. When $e^+e^- \rightarrow t\bar{t} \rightarrow b\bar{b}W^+W^- \rightarrow 6\text{-jet}$ events have been calculated (at tree-level), the following values of t - and W^\pm -parameters were adopted: $m_t = 175$ GeV, $\Gamma_t = 1.54$ GeV, $M_W = 80.23$ GeV and $\Gamma_W = 2.2$ GeV. As centre-of-mass (CM) energies representative of LEP1, LEP2 and NLC, we have used the values $\sqrt{s} = M_Z, 180$ GeV and 500 GeV, respectively.

The vertex couplings (or ‘chiral coefficients’) c_R and c_L of eq. (22) between

	γ	Z	W	g
c_R	Q^f	$g_R^f/s_W c_W$	0	1
c_L	Q^f	$g_L^f/s_W c_W$	$1/\sqrt{2}s_W$	1

Table 4: The couplings c_R and c_L of eq. (22) for u - and d -type (anti)quarks and electrons/positrons to the gauge bosons γ , Z , W and g . One has (adopting the notations $s_W \equiv \sin \theta_W$ and $c_W \equiv \cos \theta_W$) $g_R^f = -Q^f s_W^2$ and $g_L^f = T_3^f - Q^f s_W^2$ (with $q = u, d$), where $(Q^u, T_3^u) = (+\frac{2}{3}, +\frac{1}{2})$, $(Q^d, T_3^d) = (-\frac{1}{3}, -\frac{1}{2})$ and $(Q^e, T_3^e) = (-1, -\frac{1}{2})$ are the fermion charges and isospins.

quarks/leptons and gauge bosons entering in the expressions of the S , Y and Z functions can be found in Tab. 4 (we have included also the $W^\pm q\bar{q}'$ vertex, for completeness, though it will not appear in our formulae).

3 Results

We define the y -dependent six-jet fraction by means of the relation

$$f_6(y) = \frac{\sigma_6(y)}{\sum_m \sigma_m(y)} = \frac{\sigma_6(y)}{\sigma_t}, \quad (27)$$

where $\sigma_6(y)$ is the actual six-parton cross section and σ_t identifies the *total* hadronic rate $\sigma_t = \sigma_0(1 + \alpha_s/\pi + \dots)$, σ_0 being the Born cross section. In perturbative QCD one can rewrite eq. (27) in terms of a series in α_s , beginning with its fourth power, as

$$f_6(y) = \left(\frac{\alpha_s}{2\pi}\right)^4 G(y) + \dots, \quad (28)$$

where $G(y)$ is the lowest-order (or leading-order, LO) ‘coefficient function’ of the six-jet rate. We show this quantity in Fig. 4, for the case of the Durham, Cambridge and Jade schemes, at LEP1⁹. Our rates for the Jade and Durham schemes nicely match the ‘leading-order’ predictions (both in α_s and $\log(1/y)$) given in Ref. [84] in the region of $y \approx 1 \times 10^{-4}$ for the Durham scheme and when $y \approx 5 \times 10^{-4}$ for the Jade one. Here and in the following, though, we will take as a lower limit of our y -range the value of 0.001, where fixed-order perturbation theory should be much more reliable.

A salient feature of Fig. 4 is that the Jade rate is much above the Durham and Cambridge ones. At $y = 0.001$ the ratio between the former and the latter two is about 8.0. (Notice

⁹Here and in the following, unless otherwise stated, the summations over the three reactions (1)–(3) and over all possible massless combinations of quark flavours in each of these have been performed.

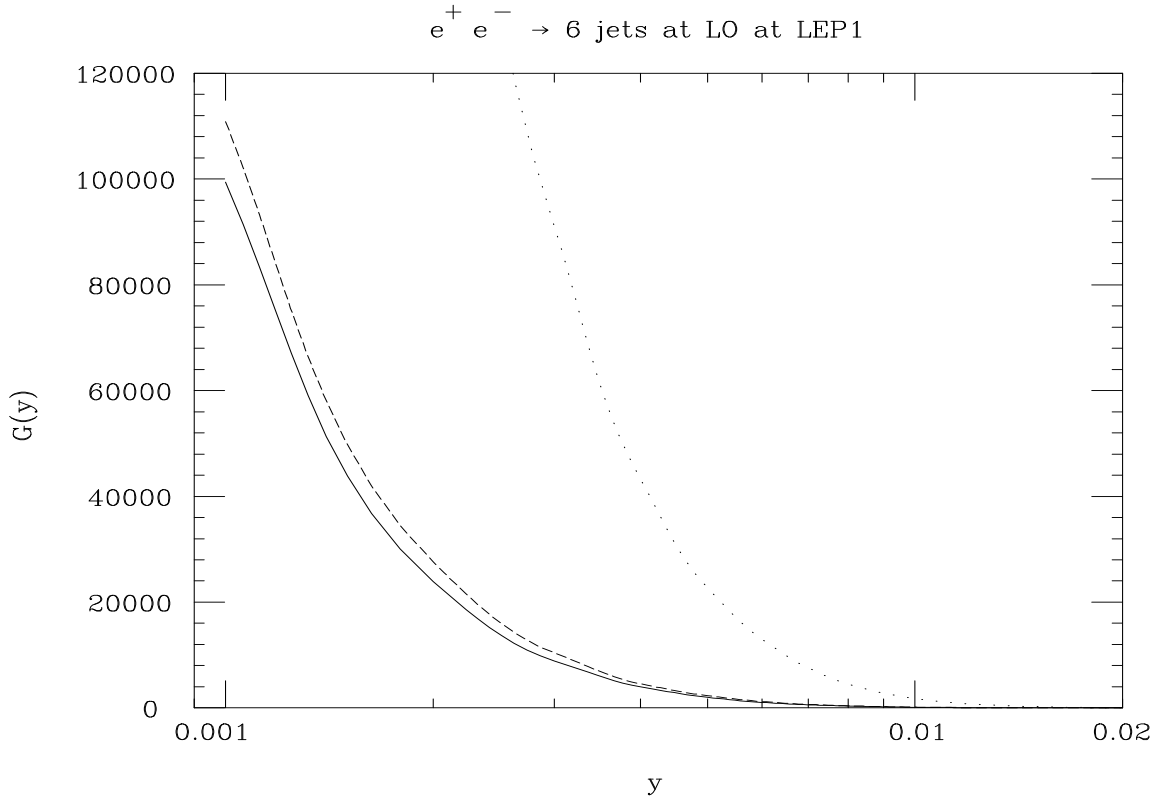


Figure 4: The parton level $G(y)$ function entering in the six-jet fraction at LO in the D (continuous line), C (dashed line) and J (dotted line) schemes, at LEP1.

that the corresponding number for the three-, four- and five-jet rates is 2.3, 3.6 and 5.7, respectively.) This effect is due to the fact that y_{ij}^J is always greater than or equal to $y_{ij}^{D,C}$, as can be easily understood from eqs. (25)–(26). Therefore, for a specified y and a given configuration of energies and angles $E_i, E_j, \cos \theta_{ij}$, more events will pass the cut $y_{ij}^{J,D,C} > y$ in the J case than in the D and C ones.

We do not push any further similar comparisons involving the J scheme. We have retained it in Fig. 4 because it has been used extensively at LEP1 in the past years. However, such algorithm has been proven to be more sensitive to hadronisation effects than the D and C algorithms, especially at low y values, where the six-jet fraction onsets [83, 85]. Furthermore, the Jade rates do not show the usual Sudakov exponentiation of multiple soft-gluon emission [38], despite having an expansion of the form $\alpha_s^n \ln^m(1/y)$ at small values of the resolution parameter, contrary to the case of the Durham and Cambridge schemes

(see [83] and references therein), and generally have a scale dependence of the fixed-order perturbative rates (e.g., the three- [85] and four-jet [86] fractions) larger than that of the D and C schemes. Thus, given the mentioned flaws, in the following we will give total and differential rates only for the last two cases¹⁰.

As for these, one should notice that the larger rate for the C scheme as compared to the D one is a direct consequence of the ‘soft freezing’ procedure of resolved jets described in Ref. [83]. The step of eliminating from the sequence of clustering the less energetic one in a resolved pair of particles (i.e., with $y_{ij}^C > y$), implemented in the C algorithm, tends to enhance the final jet multiplicity of the original D scheme. In fact, the procedure prevents the attraction of the remaining particles (at large angle) into new unresolved pairs, whose momenta would then be merged together, producing a lower number of final jets. For example, at $y = (0.001)[0.005]\{0.010\}$, relative differences between the two algorithms are of the order of (10)[14]{16} %.

The jet fraction $f_6(y)$ and cross section $\sigma_6(y)$ corresponding to the rates in Fig. 4 are given in Tab. 5, for a representative selection of y ’s. The value of α_s adopted is 0.120, whereas that used for σ_t is 39.86 nb. Given the total luminosity collected at LEP1 in the 1989-1995 years (more than 10^7 hadronic events have been recorded by the four Collaborations), the six-jet event rate is comfortably measurable. For example, for a luminosity of, say, 100 pb⁻¹ per experiment, perturbative QCD predicts at LO some 58,000 original six-parton events recognised as six-jet ones, for $y = 0.001$ in the C scheme (a number that decreases to approximately 52,000 if the D algorithm is adopted instead).

The rates given in Figs. 4 and Tab. 5 are LO results. Next-to-leading order (NLO) corrections proportional to $\mathcal{O}(\alpha_s^5)$ are expected to be large. In fact, the size of higher-order (HO) contributions generally increases with the power of α_s and with the number of particles in the final state or, in other terms, with their possible permutations (i.e., with the number of different possible attachments of both the additional real and virtual particles to those appearing in lowest order). As already mentioned, the highest-order corrections calculated to date in $e^+e^- \rightarrow n$ -jet annihilations are the NLO ones to the four-jet rate, that is, terms proportional to α_s^3 [13, 14]. The total four-jet cross section at NLO was found to be larger than that obtained at LO in α_s^2 by a K-factor of 1.5 or more, depending on the value of y implemented during the clustering procedure and the algorithm used as well. Therefore, we should expect that the rates given in Tab. 5 underestimate the six-jet rates by *at least* a similar factor. Indeed, assuming a $K \approx 2$ correction, our results are in a satisfactory agreement with both data and phenomenological Monte Carlo (MC) programs [87].

¹⁰Apart from one example, when we will need to compute a cross section using the J scheme for purpose of comparison against results published in literature.

y	$f_6(y)$	$\sigma_6(y)$ (pb)
0.001	$(1.31)[1.47] \times 10^{-2}$	$(523.91)[584.19]$
0.002	$(3.16)[3.65] \times 10^{-3}$	$(125.95)[145.44]$
0.003	$(1.17)[1.37] \times 10^{-3}$	$(46.81)[54.72]$
0.004	$(5.29)[6.01] \times 10^{-4}$	$(21.09)[23.96]$
0.005	$(2.63)[3.05] \times 10^{-4}$	$(10.49)[12.17]$
0.006	$(1.38)[1.59] \times 10^{-4}$	$(5.49)[6.35]$
0.007	$(7.90)[8.85] \times 10^{-5}$	$(3.15)[3.53]$
0.008	$(4.80)[5.20] \times 10^{-5}$	$(1.91)[2.07]$
0.009	$(2.77)[3.08] \times 10^{-5}$	$(1.10)[1.23]$
0.010	$(1.64)[1.93] \times 10^{-5}$	$(0.65)[0.77]$
LEP1		

Table 5: Jet fraction and cross section rates for $e^+e^- \rightarrow 6$ jets at LEP1, for several values of y in the Durham and Cambridge schemes, in round and squared brackets, respectively. The numerical errors do not affect the significant digits shown.

In this respect the MCs [88]–[92] largely exploited in experimental analyses apparently perform better than the fixed-order perturbative calculations, especially at low y -values, where the latter need to be supported by the additional contribution of perturbation series involving powers of $\log(1/y)$ resummed to all orders (for the case of the D and C scheme, see Refs. [39, 40, 83]) in order to fit the same data. However, as such MCs generally implement only the infrared (i.e., soft and collinear) dynamics of quarks and gluons in the standard ‘parton-shower (PS) + $\mathcal{O}(\alpha_s)$ Matrix Element (ME)’ modelling, in many cases their description of the large y -behaviour and/or that of the interactions of secondary ‘branching products’ is (or should be expected to be) no longer adequate. In fact, this has been shown to be the case, e.g., for some typical angular quantities of four-jet events [47, 93]. As discussed in Ref. [94], these differences are presumably due to a poor description of the spin correlations among the various partons implemented in the MCs: in particular, between the primary (i.e., from the $\gamma^*, Z^{(*)}$ -splitting) and secondary (i.e., from the gluon splitting into gluons or quarks) pairs. In contrast, once $\mathcal{O}(\alpha_s^2)$ MEs are inserted and properly matched to the hadronisation stage, e.g., using the JETSET string fragmentation model [90] (see also Ref. [95]), then the agreement is recovered¹¹. If one considers that four-jet events

¹¹In this context, one should however mention that ME models with ‘added-on’ fragmentation, i.e., ‘ $\mathcal{O}(\alpha_s^2)$ + hadronisation’ cannot be reliably extrapolated from one energy to another, as the fragmentation tuning is energy dependent. To obviate this, a special ‘ $\mathcal{O}(\alpha_s^2)$ + PS + cluster hadronisation’ version of HERWIG is

represent only the next-to-lowest-order QCD interactions in e^+e^- scatterings, then it is not unreasonable to argue that further complications might well arise as the final state considered gets more and more sophisticated, such as in six-jet events.

In order to emphasise this point, we present in Figs. 5–6 the differential distributions of the six-jet rate (along with the five- and four-jet ones) in some typical shape variables used in QCD studies in electron-positron annihilations. They are the thrust T [97], the oblateness O [98], the C-parameter C [99], the heavy M_H , light M_L and difference M_D jet masses [100], the sphericity S , aplanarity A and planarity P [101], the minor m and major M values [98] and the D-parameter [99]. (Their allure in testing the underlying QCD dynamics has been well illustrated in, e.g., Ref. [32].) In Figs. 5–6 the algorithm used to produce the plots was the Cambridge one, with $y = 0.001$.

As compared to the same distributions in the case of lower jet multiplicity events (such as, e.g., four-jet production), those in Figs. 5–6 for the six- (more markedly) and five-jet (in some instances) rates are much more ‘central’. That is, the peaks of the distributions are generally further away from the infrared regions, those which dominate the phenomenology of n -jet events, for $n = 3$ and 4. (The only exception is the C-parameter, which is indeed expected to play a rôle apart since there exists a singularity at the boundary of the three-parton phase space $C = 2/3$, see Ref. [102], affecting the four-jet distribution but not the five- and six-jet ones.) This is a clear indication that other dynamics (other than the soft and collinear emission of gluons off quark lines) has a perceptible influence on differential jet rates, as the multiplicity of the latter increases. In other terms, one should expect the above mentioned spin correlations among the partons to modify quite significantly the infrared behaviour dictated by the propagators when the energy of the particles decreases, as happens in the six-parton case and particularly for the secondary and tertiary branching products of the $g \rightarrow q\bar{q}$, $g \rightarrow gg$ and $g \rightarrow ggg$ splittings (see Fig. 1).

To further stress this, we also plot in Figs. 5–6 the same shape variables distributions as obtained at hadron level for the six-jet (i.e., $n = 6$) rate by using the HERWIG event generator, with identical choice of jet algorithm and resolution as above. As a matter of fact, the MC spectra depart in most cases quite substantially from those obtained by using the exact $\mathcal{O}(\alpha_s^4)$ MEs, notably, they ‘point’ towards the singularities. Such behaviour is particular evident for thrust and sphericity, two variables to which we will come back below.

Under these circumstances, we believe the availability of exact perturbative calculations of six-jet events to be essential in order to model correctly the HO parton dynamics for both future tests of QCD (like those outlined here) and QCD background studies (as we will show later on for the case of $t\bar{t} \rightarrow 6$ -jet production and decay at NLC).

now in preparation [96].

The total hadronic cross section falls drastically when increasing the CM energy from the LEP1 to the LEP2 values, by more than three orders of magnitude, and so does the six-jet rate. Nonetheless, six-jet fractions have been measured also during the 1995-1996 runs at the CM energies of 130–136, 161 and 172 GeV, when a total luminosity of around 27 pb⁻¹ was collected, and are currently under further investigation (at 183 GeV and higher). Results can be found for the lower energies in Ref. [103]. Within a ‘typical’ K-factor of 2 (which tentatively quantifies the ratio between the NLO and the LO six-jet rates also at LEP2) the values of $f_6(y)$ as reconstructed from our rates are always well compatible with those produced by the MCs used by e.g., the ALEPH Collaboration [104]. (Notice that this is also true at $\sqrt{s} = 161$ GeV, where a six-jet ‘excess’ has apparently been observed [104]). For reference, we present the jet rates at $\sqrt{s} = 180$ GeV in Fig. 7 in the form of the total cross section. The relative differences between the two D and C algorithms are similar to those already encountered at LEP1.

Quite apart from its relevance in QCD jet fractions, the six-jet rate at LEP2 can in principle represent a source of background to the so called ‘colour reconnected’ W^+W^- hadronic decays [105]. The problem goes as follows. Colour exchange (both at perturbative and non-perturbative level) can take place between the decay products of the two W^\pm ’s, thus destroying the notion of two separate W^\pm decays and hence casting doubts on our abilities to reconstruct accurately the mass of the resonances. In perturbative terms, such effect is due to the presence of interference terms in the total cross section for $W^+W^- \rightarrow$ multi-parton production and decay, which account for the exchange of real or virtual partons emitted in the decay of one of the W^\pm ’s and absorbed by the partons generated by the other. Simple rules of colour conservation show that such colour effects cannot occur at first order in α_s , but only in higher orders (i.e., at least two gluons need to be exchanged). At the non-perturbative level, a similar phenomenon takes place when the colour strings generated among the partons from the first W^\pm decay overlap with those from the second one, break down and form new strings which may join quarks from different shower cascades (e.g., in the language of the Lund fragmentation model [106]). Of the two contributions, the non-perturbative one is expected to be dominant [107]. The consequence is similar at both levels: namely, particles are generated that cannot be unambiguously assigned to one W^\pm decay or another.

It is of decisive importance to quantify accurately the above effects, especially if one wants to achieve a high precision measurement of the mass M_W of the W^\pm boson (a target accuracy of $\pm(40 - 50)$ MeV or less is expected, see, e.g., Ref. [108]). In fact, at present, their dynamics is relatively unknown. On the one hand, a complete $\mathcal{O}(\alpha_s^2)$ perturbative calculation of W^+W^- production and decay does not exist to date, as only the tree-level part of $e^+e^- \rightarrow W^+W^- \rightarrow 6$ jets has been computed so far [58]. On the other hand, in the

non-perturbative modelling, many more additional parameters are needed to describe the reconnection effects than the well tested mechanisms of the quark and gluon fragmentation, so that there are many phenomenological programs now on the market, indeed predicting rather different sizes for the above colour effects [109].

Whereas the treatment of non-perturbative colour rearrangement effects is beyond the scope of the paper, we come back to the perturbative ones. In particular, we would like to recall that Ref. [58] gave an estimate of the size of the latter at LO, in the form of the part of the $e^+e^- \rightarrow W^+W^- \rightarrow 6\text{-jet}$ cross section due to the mentioned interference terms. The effect was found to be quite small: e.g., at the level of $\approx 4 \times 10^{-3}$ pb at $y = 0.001$ for the Jade algorithm, with $\sqrt{s} = 175$ GeV and using $\alpha_s = 0.115$. The cumulative rates for processes (1)–(3) for the same jet clustering scheme and the identical combination of y , \sqrt{s} and α_s amount to approximately 2 pb, well above the colour reconnected rates in $W^+W^- \rightarrow 6\text{-jet}$ events. Since in the latter case colour exchange proceeds via gluons, in Ref. [58] the corresponding energy spectra were studied, in order to give some hints about the sort of energy at which perturbative colour reconnection takes place. The softest gluon energy distribution was found to peak at about 8 GeV, whereas that of the most energetic one lies at approximately 20 GeV. To a good degree of approximation, the two gluon energy spectra coincide with those of the two least energetic particles in $W^+W^- \rightarrow 6\text{-jet}$ decays. In Fig. 8, we have studied the energy spectra of the partons produced via reactions (1)–(3). Coincidentally enough, the fifth and the fourth most energetic ones show their maxima around 8 and 20 GeV, respectively¹². That is, they behave on the same footing as the gluon jets in $e^+e^- \rightarrow W^+W^- \rightarrow 6\text{-jet}$ events, which are responsible for perturbative colour rearrangement. Though both the studies in Ref. [58] and those presented here need to be eventually supported by loop-calculations as well, it is clear that six-jet events from QCD represent a considerable source of irreducible background to hadronic W^+W^- events perturbatively reconnected.

As a matter of fact, one might consider imposing a cut such as $M_{jj} \approx M_W$, that is, asking that one di-jet invariant mass (see below, eq. (29)) is close to the value of the W^\pm mass, as one might naively expect to occur naturally in $W^+W^- \rightarrow 6\text{-jet}$ events. However, this could well be counter-productive, for two reasons. Firstly, the colour reconnected contribution to $e^+e^- \rightarrow W^+W^- \rightarrow 6\text{-jet}$ events is defined as the sum of two terms, namely, the interference between the set of diagrams labelled (A1) and (A2) plus that between (A3) and (A4) in Fig. 9¹³. (Note that the cross term between (A1)⊕(A2) and (A3)⊕(A4) is identically

¹²Further notice that also in events of the type (1)–(3) the fifth and fourth most energetic partons are in most cases gluons, because of the dominance in the total QCD cross section of two-quarks-four-gluon events, with the two fermion being the most energetic ones.

¹³We would like to thank the authors of Ref. [58] for their kind permission of exploiting here one of the

zero). Neither of the two terms has a distinctive peak at $M_{jj} \approx M_W$, in line with the notion of colour exchange taking place between the two W^\pm decays. Secondly, the invariant mass of the di-jet combination formed by pairing the first and third most energetic jets from six-jet QCD events peaks not far from the W^\pm mass, i.e., at ≈ 76 GeV (less than two Γ_W from M_W) and is rather broad in the region $M_{jj} \approx M_W$, as can be appreciated in Fig. 10 (here, our default algorithm, resolution parameter and CM energy for LEP2 have been used again, as the shape of the distribution is not significantly affected by either of those, provided $\sqrt{s} \gg 2M_W$ for the energy). Further notice that other QCD di-jet mass distributions populate the region around the M_W resonance, such as the combinations $ij = 12, 14$ and 23 (the other spectra are much softer, as they concentrate at low invariant masses). Evidently then, under these circumstances, our understanding of perturbative colour interconnection effects in $W^+W^- \rightarrow 6\text{-jet}$ decays is bound to our ability in suppressing the corresponding QCD background. This operation can however be attempted only in the context of a detailed Monte Carlo simulation, including parton shower, hadronisation and detector effects, which is beyond our capabilities.

The six-jet event rate that will be collected at NLC can be rather large, despite the cross section being more than a factor 10^4 smaller than at LEP1 (e.g., at $\sqrt{s} = 500$ GeV). This is due to the large yearly luminosity expected at this machine, around 10 fb^{-1} . For such a value and assuming a standard evolution of the coupling constant with the increasing energy (that is, no non-Standard Model thresholds occur up to 500 GeV), at the minimum of the y -values considered here (i.e., $y = 0.001$), one should expect some 220 events per annum by adopting the D scheme and about 13% more if one adopts the C one. However, these rates decrease rapidly as the resolution parameter gets larger, by a factor of 50 or so at $y = 0.005$ and of approximately 800 at $y = 0.01$.

It is also interesting to look at the composition of the total rates in terms of the three processes (1)–(3). Whereas this is probably of little concern at LEP1 and LEP2, the capability of the detectors of distinguishing between jets due to quarks (and among these, bottom flavours in particular: e.g., in tagging top and/or Higgs decays) and gluons, is essential at NLC, in order to perform dedicated searches for old and new particles. The separate behaviours of the reactions in (1)–(3) can be appreciated in Fig. 11, e.g., for the case of the C scheme, in terms of total cross sections. The rates for the D algorithm follow the same pattern.

The tagging of b -quarks produced, e.g., in the hadronic top decay chain $t\bar{t} \rightarrow b\bar{b}W^+W^- \rightarrow b\bar{b}jjjj$, is of decisive importance, non only to suppress the QCD background (mainly proceeding via gluon events, see Fig. 11) but also to reduce the combinatorics in-

volved in selecting three jets out of six, in case no flavour identification is exploited (twenty combinations in total). If b -quark jets can be recognised (via their semileptonic decays, via μ -vertex devices, etc.), then only six three-jet combinations bjj (or $\bar{b}jj$) need to be selected, one of which is such that $M_{bjj(\bar{b}jj)} \approx m_t$. If ϵ_b is the efficiency of tagging one single b -jet within a certain fiducial volume, and two taggings are required, then ϵ_b^2 is the overall rate for identifying events containing exactly two b -quarks (we assume no correlations between the two b -taggings and that the charge of the heavy quark is recognised). This is the case which applies to the subprocesses $e^+e^- \rightarrow b\bar{b}gggg$ and $e^+e^- \rightarrow b\bar{b}q\bar{q}q'\bar{q}'$ (with $q, q' \neq b$)¹⁴. The probability of misidentifying six-jet events produced via four- b -quark reactions (i.e., $e^+e^- \rightarrow b\bar{b}b\bar{b}gg$ or $e^+e^- \rightarrow b\bar{b}b\bar{b}q\bar{q}$ (with $q \neq b$)) as $b\bar{b}jjjj$ events is then $[2\epsilon_b(1 - \epsilon_b)]^2$. If there are six b -quarks in the event, as in $e^+e^- \rightarrow b\bar{b}b\bar{b}b\bar{b}$, then the corresponding number is $[3\epsilon_b(1 - \epsilon_b)]^3$. The total rates as a function of y in the C scheme for six-parton process involving b -quarks are given in Fig. 12, for the case in which only u and d massless contributions are considered (for c and s , respectively, one gets very similar results, even when the masses, e.g., $m_c = 1.35$ GeV and $m_s = 0.30$ GeV, are retained in the calculation).

If one multiplies the rates given in Fig. 12 by the overall b -tagging efficiencies mentioned in the previous paragraph, then one realises that six-jet events produced via four- and six- b -quarks subprocesses yield negligible rates at NLC (assuming, e.g., $\epsilon_b = 70\%$, the current LEP value). Events involving only two b -quarks can instead produce a detectable number of $b\bar{b}jjjj$ events, especially at low y . For example, for $y = 0.001$ in the C scheme one gets some 15 QCD background events in $b\bar{b}jjjj$ samples (including the b -tagging efficiency ϵ_b^2), after a luminosity of ten inverse femtobarns has been collected. Though this is not a large number per se, considering that $e^+e^- \rightarrow t\bar{t} \rightarrow 6$ jets yields about 800 doubly b -tagged events at the same y -value in the above scheme, one should recall that very high precision measurements of top parameters (such as m_t , Γ_t , the branching ratios, etc.) are expected to be carried out at NLC [110]. Under these circumstances, even small backgrounds need to be quantified accurately.

Whereas mass effects (markedly, of b -quarks) are always negligible (at LEP1, LEP2 and also NLC) if the sum over all flavour combinations is performed (that is, when no heavy flavour tagging is exploited), they can in principle be important in b -jet samples, as in those selected for top studies at NLC. As a matter of fact, in the individual contributions to the six-jet rate mass corrections can be quite sizable at $\sqrt{s} = 500$ GeV, as shown in

¹⁴For simplicity, we do not consider here the case of c -quark misidentified as b -quarks. We can presumably assume that by the time NLC will be operative the efficiency in distinguishing between c - and b -quark jets will be much higher than at present. The rejection factor against light quark jets (produced by u -, d - and s -quarks) as well as against gluon jets is very high already at present, so that we do not need to worry about their contamination in the present analysis.

Fig. 12, at the level of ten percent or more. These corrections are more visible when more b -quarks are produced in the final state. However, as previously mentioned, these multi- b -quark subprocesses are unlikely to be important in top analyses. In practise, the largest part of the $b\bar{b}jjjj$ sample produced from QCD comes from two-quark-four-gluon events, where b -mass effects are naturally smaller because only two massive particles are involved, over a six-particle phase space and at rather high energy ($\sqrt{s} \gg 2m_b$). In the end, b -mass effects on the complete $b\bar{b}jjjj$ produced by QCD amount to only 4% at the NLC, for typical values of the resolution parameter in the six-jet region, $y \approx 0.001$. We have also verified that the differential distributions (e.g., energy and angles) suffer imperceptibly from mass corrections, so is the case of the shape variable spectra. Therefore, in first instance, it is safe to assume the value $m_b = 0$ in numerical simulations of QCD six-jet events. We will do so in the remainder of the paper.

The concern about possible background effects at the NLC due to six-jet events from pure QCD comes about if one further considers that they may naturally survive some of the top signal selection criteria. These can in fact rely on the analysis of shape variable spectra of six-jet samples, in particular, the thrust and sphericity distributions, and since the latter (as already mentioned while commenting Figs. 5–6) might well be poorly described by the parton shower approach exploited in the phenomenological MC programs, it is of decisive importance that also the non-infrared dynamics of events of the type (1)–(3) is carefully studied.

It is well known that the large value of the top mass leads to rather spherical signal events. Therefore, shape variables such as the two mentioned above represent useful means to disentangle $e^+e^- \rightarrow t\bar{t}$ events. For example, a selection strategy that does not exploit neither lepton identification nor the tagging of b -jets was outlined in Ref. [111]. This approach has a twofold attractiveness: firstly, its simplicity; secondly, it is a rather general procedure, that can be equally applied both at and above the threshold $\sqrt{s} \approx 2m_t$. The requirements are a large particle multiplicity, a high number of jets (at least five, eventually forced to six by a clustering scheme) and a rather low thrust (typically, below 0.85). Jets are selected according to a jet clustering algorithm (in our case, the Cambridge one with $y = 0.001$, for sake of illustration).

Clearly, the six-jet events meet the two first criteria. As for the thrust and sphericity distributions, these are shown in Fig. 13. From there it is evident the overlapping of the two distributions ($t\bar{t}$ and QCD events) in the region where the signal events are mostly located, for both thrust and sphericity. A cut such as that advocated in Ref. [111], i.e., $T < 0.85$, would then be rather ineffective against six-jet events from QCD. Once again, we believe that a correct modelling of the phenomenology of the latter based on a ME description will be essential to quantify correctly the effects of the QCD background, especially in view of

the mentioned high precision measurements of top parameters.

Tests of multiple electroweak self-couplings of gauge-bosons (as well as searches for new resonances) at NLC will often need to rely on the mass reconstruction of multi-jet systems (particularly di-jet ones). Therefore, it is instructive to look at the invariant mass distributions which will be produced by all the possible two-parton combinations ij in six-jet events from QCD at $\mathcal{O}(\alpha_s^4)$ (with $i = 1, \dots, 5$ and $j = i + 1, \dots, 6$). As usual in multi-jet analyses, we first order the jets in energy, so that $E_1 > E_2 > \dots > E_5 > E_6$. Then, we construct the quantities (the equality strictly holds only for massless partons ij , as is the case here)

$$m_{ij} \equiv \frac{M_{ij}^2}{s} = \frac{2E_i E_j (1 - \cos \theta_{ij})}{s}, \quad (29)$$

where M_{ij}^2 represents the Lorentz invariant (squared) mass. These fifteen quantities are shown in Fig. 14 for the C scheme at $y = 0.001$, their shape being similar for the D algorithm. We found it convenient to plot the ‘reduced’ invariant masses m_{ij} rather than the actual ones M_{ij} , as energies and angles ‘scale’ with the CM energy in such a way that the shape of the distributions is largely unaffected by changes of the value of \sqrt{s} in the energy range relevant to NLC. Therefore, from Fig. 14 one should then be able to reconstruct rather accurately the Lorentz invariant mass distributions for a given CM energy \sqrt{s} by exploiting eq. (29). Note that the reduced mass spectra are similar in all three reactions (1)–(3), their integral being however rescaled according to the numbers given in Fig. 11. To allow for an easy conversion of the differential cross sections into numbers of events in a certain mass range, the spectra in Fig. 14 sum to the total cross section of processes (1)–(3) at NLC.

It is interesting to notice in Fig. 14 the ‘resonant’ behaviour of some of the distributions. This is particularly true for those involving the most energetic of all the partons. Using the definition (29) they translate into peak-like structures at the true invariant mass values $M_{ij} \approx (250)[212]\{177\}$ GeV, for the combinations $ij = (12)[13]\{14\}$, and, possibly, $M_{15} \approx 150$ GeV as well. In all the other cases the spectra are generally softer and do not show any distinctive kinematic feature. Once again, it is important that all such behaviours are correctly implemented in the simulation programs that will be adopted by the NLC experiments, so that it will be possible to recognise and eventually subtract the six-jet QCD background.

A further general comment that is in order for six-parton QCD events produced at NLC is that the much lower value of α_s at those high energies (as compared to that at LEP1 and/or LEP2) in principle implies a reduced importance of the uncalculated HO strong corrections, so that the theoretical uncertainty on the rates of processes (1)–(3) will be more under control at the future collider than it was/is at the energy scales of the two LEP phases.

So far we not included effects of ISR in any of our calculations for six-jet production. However, it is well known [53] that photon bremsstrahlung generated by the incoming electron and positron beams can be quite sizable at NLC. In contrast, at LEP1 and LEP2 such radiation is suppressed by the width of the Z and W^+W^- resonances, respectively¹⁵. In order to implement ISR we resort to the mentioned ESF approach. In particular, we use the expressions given in Ref. [114], through the order α_{em}^2 . We plot the production rates for the sum of the processes (1)–(3) in presence of ISR in Fig. 15, as a function of the resolution parameter y in the C scheme. (Effects turn out to be similar in the D scheme.) They are compared to those obtained without ISR (that is, the sum of the rates in Fig. 11). No cut is here applied to the soft and collinear photons from the initial state. We see that the curve corresponding to the processes (1)–(3) convoluted with ISR lies above the lowest-order one. This is rather intuitive, as it is well known that the radiation of photons from the incoming electron and positrons tends to lower the ‘effective’ CM energy of the collision [113]. Since processes (1)–(3) proceed via s -channel diagrams, the expected overall effect would be an enhancement of the total rates. In fact, this is what can be seen in Fig. 15. At $y = 0.001$, the difference is around 25% and this tends to increase as y gets larger. However, we have verified that the shape of the differential distributions (such as those in shape variables, see Fig. 13, and in invariant mass, see Fig. 14) suffer little from ISR effects.

As announced in the Introduction, we also devote some space to analyse photoproduction in 5jet + 1γ , 4jet + 2γ , 3jet + 3γ and 2jet + 4γ events. For this study, we reconsider the case of LEP1 energies, where the impact of ISR is much less relevant than at LEP2 and NLC (recall that we did not implement the resummed logarithmic part of it in photonic events). In the first two cases we consider both the dominant contributions involving only two quarks and the suppressed ones involving four, whereas in the last two cases only two quarks can participate in the event.

Final states including photons are actively studied experimentally in order to determine the electroweak couplings of the quarks and as a mean to search for new phenomena [115]. Furthermore, such particles are the only ones which can be directly revealed and couple to the quarks at each stage of the perturbative parton shower (see Fig. 1), so that the detection of hard isolated photons (or ‘direct photons’) is extremely useful for a detailed understanding of the underlying partonic picture as well as of the QCD evolution from large to small energy scales. (Conversely, soft photons lying close to hadronic tracks can give information about the parton fragmentation mechanisms, though the corresponding rates are not calculable

¹⁵In addition, peculiar features at NLC is the presence of Linac energy spread and beamsstrahlung [112]. However, their effects are negligible, as compared to those produced by ISR, at least for the ‘narrow’ D-D and TESLA collider designs [113]. For this reason, we do not consider them in our analysis. They would however be straightforward to insert.

perturbatively.) In particular, the more jets are separated in association with photons, the more likely will be that photons were radiated by quarks in later stages of such evolution. In $e^+e^- \rightarrow m \text{ jet} + n \text{ photon}$ events (with $m+n=6$ and $m \geq 2$), γ -radiation always takes place from the primary quark-antiquark pair (i.e., that produced in the γ, Z -splitting) in the case of the dominant two-quark events. Thus, for the cases $m=4(5)$ and $n=2(1)$, such contributions should be regarded as a source of background in the mentioned analyses, with the four-quark contributions being the interesting ones, as in these cases photons can also be radiated by secondary branching products.

In this study, we limit ourselves to giving some total rates. The cross sections for isolated photon events as a function of the y resolution parameter, applied to both quarks/gluons and photons on the same footing (in the spirit of the so-called ‘democratic approach’ [116]), in the C scheme, are presented in Fig. 16, at LEP1. The mentioned cuts in transverse momentum and polar angle of the photons have been enforced, in order to screen the singularities due to infrared (i.e., soft and collinear) EM emission from electrons and positrons. The hierarchy in the cross sections of Fig. 16 is dictated mainly by the perturbative order $\mathcal{O}(\alpha_{em}^{m+2}\alpha_s^n)$ for the hard production of m jets and n photons. At LEP1, given, e.g., some 400 inverse picobarn of total accumulated luminosity, one should expect that only the 5jet + 1 γ and 4jet + 2 γ events can yield an observable rate, with the four-quark contributions being roughly one order of magnitude smaller than the two-quark ones in both cases.

4 Summary

In summary, we have studied at the partonic level the tree processes $e^+e^- \rightarrow q\bar{q}gggg$, $e^+e^- \rightarrow q\bar{q}q'\bar{q}'gg$ and $e^+e^- \rightarrow q\bar{q}q'\bar{q}'q''\bar{q}''$ (for massless and massive quarks) at leading-order in perturbative QCD, by computing their exact matrix elements. The latter task has been accomplished thanks to the use of spinor techniques and colour decomposition methods. Both the formulae for the Feynman amplitudes and the relevant QCD (i.e., for $N_C=3$) colour factors have been given explicitly. Several phenomenological applications at present and future colliders have been discussed. Two **FORT**RAN codes have been produced and cross checked with each other on several different platforms: VMS, OSF, HP. The fastest of the two requires about 3×10^{-3} CPU seconds to evaluate a single event on an alpha-station DEC 3000 - M300X, which makes it suitable for high statistics Monte Carlo simulations. Further optimisations are, however, in progress.

5 Acknowledgements

We acknowledge the UK PPARC support. We thank the Theoretical Physics Groups in Fermilab and Lund for their kind hospitality while part of this work was carried out. This research work was supported in part by the Italian Institute of Culture ‘C.M. Lerici’ under the grant Prot. I/B1 690, 1997. Finally, we are grateful to David J. Miller for carefully reading the manuscript and for several useful discussions and comments.

References

- [1] R.K. Ellis, W.J. Stirling and B.R. Webber, “QCD and Collider Physics” (Cambridge University Press, 1996).
- [2] M.L. Mangano and S.J. Parke, *Phys. Rep.* **200** (1991) 301.
- [3] R. Gastmans and T. T. Wu, “The ubiquitous photon” (Addison Wesley, 1990).
- [4] F. Bloch and A. Nordsieck, *Phys. Rev.* **52** (1937) 54.
- [5] T. Kinoshita, *J. Math. Phys.* **3** (1962) 650;
T.D. Lee and M. Nauenberg, *Phys. Rev.* **133** (1964) 1549.
- [6] G. Sterman, *Phys. Rev.* **D17** (1978) 2789.
- [7] See, e.g.:
L. M. Brown and R. P. Feynman, *Phys. Rev.* **85** (1952) 231;
D. B. Melrose, *Il Nuovo Cimento* **40A** (1965) 181;
A.C.T. Wu, *Mat. Fys. Medd. Dan. Vid. Selsk.* **33** No. 3 (1961) 72;
G. Passarino and M. Veltman, *Nucl. Phys.* **B160** (1979) 151;
G. ’t Hooft and M. Veltman, *Nucl. Phys.* **B153** (1979) 365;
W. van Neerven and J.A.M. Vermaseren, *Phys. Lett.* **B137** (1984) 241;
G.J. Van Oldenborgh and J.A.M. Vermaseren, *Z. Phys.* **C46** (1990) 425;
A. Denner, U. Nierste and R. Scharf, *Nucl. Phys.* **B367** (1991) 637;
A. Denner, *Fort. Phys.* **41** (1993) 307;
U. Nierste, D. Müller and M. Böhm, *Z. Phys.* **C57** (1993) 605.
- [8] See, e.g.:
Z. Bern, L. Dixon and D.A. Kosower, *Nucl. Phys.* **B425** (1994) 217. *Nucl. Phys. Proc. Suppl.* **51C** (1996) 243; *Ann. Rev. Nucl. Part. Sci.* **46** (1996) 109; *Nucl. Phys. B, Proc. Suppl.* **39BC** (1995) 146;

- Z. Bern, L. Dixon, D.C. Dunbar and D.A. Kosower, *Nucl. Phys.* **B435** (1995) 59; talk presented at ‘Continuous Advances in QCD’, Minneapolis, Feb. 18-20, 1994, preprint SLAC-PUB-6490, May 1994, [hep-ph/9405248](#); talk presented at ‘DIS ’97’, Chicago, IL, April 14-18, 1997, preprint Saclay-SPhT/T97-62, June 1997, [hep-ph/9706447](#).
- [9] N.K. Falck, D. Graudenz and G. Kramer, *Phys. Lett.* **B220** (1989) 299; *Nucl. Phys.* **B328** (1989) 317;
K. Hagiwara and D. Zeppenfeld, *Nucl. Phys.* **B313** (1989) 560;
F.A. Berends, W.T. Giele and H. Kuijf, *Nucl. Phys.* **B321** (1989) 39.
- [10] R.K. Ellis, D.A. Ross and A.E. Terrano, *Nucl. Phys.* **B178** (1981) 421.
- [11] See, e.g.:
F. Mandl and G. Shaw, “Quantum Field Theory” (John Wiley & Sons, 1993).
- [12] S. Moretti, *Phys. Lett.* **B420** (1998) 367.
- [13] E.W.N. Glover and D.J. Miller, *Phys. Lett.* **B396** (1997) 257;
J.M. Campbell, E.W.N. Glover and D.J. Miller, *Phys. Lett.* **B409** (1997) 503.
- [14] Z. Bern, L. Dixon, D.A. Kosower and S. Weinzier, *Nucl. Phys.* **B489** (1997) 3;
Z. Bern, L. Dixon, D.A. Kosower, *Nucl. Phys.* **B513** (1998) 3;
A. Signer, talk presented at XXXIInd Rencontres de Moriond: QCD and High-Energy Hadronic Interactions, Les Arcs, France, 22-29 March 1997, preprint SLAC-PUB-7490, May 1997, [hep-ph/9705218](#);
L. Dixon and A. Signer, *Phys. Rev.* **D56** (1997) 4031.
- [15] W. Bernreuther, A. Brandenburg and P. Uwer, *Phys. Rev. Lett.* **79** (1997) 189;
A. Brandenburg and P. Uwer, *Nucl. Phys.* **B515** (1998) 279;
G. Rodrigo, *Nucl. Phys. Proc. Suppl.* **54A** (1997) 60;
G. Rodrigo, A. Santamaria and M. Bilenky, *Phys. Rev. Lett.* **79** (1997) 193;
P. Nason and C. Oleari, *Nucl. Phys.* **B521** (1998) 237.
- [16] B.L. Ioffe, *Phys. Lett.* **B78** (1978) 277.
- [17] G. Branco, K.H. Streng and H.P. Nilles, *Phys. Lett.* **B85** (1979) 269.
- [18] A. Ali, J.G. Körner, Z. Kunszt, E. Pietarinen, G. Kramer, G. Schierholz and J. Willrodt, *Nucl. Phys.* **B167** (1980) 454;
J.G. Körner, G. Schierholz and J. Willrodt, *Nucl. Phys.* **B185** (1981) 365.
- [19] K.J.F. Gaemers and J.A.M. Vermaseren, *Z. Phys.* **C7** (1980) 81.

- [20] O. Nachtmann and A. Reiter, *Z. Phys.* **C16** (1982) 45.
- [21] D. Danckaert, P. de Causmaecker, R. Gastmans, W. Troosts and T.-T. Wu, *Phys. Lett.* **B114** (1982) 203.
- [22] L. Clavelli and G.V. Gehlen, *Phys. Rev.* **D27** (1983) 1495.
- [23] F.A. Berends, P.H. Daverveldt and R. Kleiss, *Phys. Lett.* **B148** (1984) 489; *Nucl. Phys.* **B253** (1985) 441.
- [24] E. Laermann, K.H. Streng and P.M. Zerwas, *Z. Phys.* **C3** (1980) 289.
- [25] J. Jersák, E. Laermann and P.M. Zerwas, *Phys. Rev.* **D25** (1982) 1218.
- [26] E.W.N. Glover, R. Kleiss and J.J. van der Bij, *Z. Phys.* **C47** (1990) 435.
- [27] E.N. Argyres, C.G. Papadopoulos and S.D.P. Vlassopoulos, *Phys. Lett.* **B237** (1990) 581.
- [28] G. Kramer and B. Lampe, *Fort. Phys.* **37** (1989) 161.
- [29] A. Ballestrero, E. Maina and S. Moretti, *Phys. Lett.* **B294** (1992) 425; *Nucl. Phys.* **B415** (1994) 265; Proceedings of the XXIXth Rencontres de Moriond: QCD and High Energy Hadronic Interactions, Méribel, Savoie, France, March 1994, ed. by J. Trân Thanh Vân, ed. Frontières, Gif-sur-Yvette, 1994, 367.
- [30] A. Ballestrero and E. Maina, *Phys. Lett.* **B323** (1994) 53.
- [31] W.T. Giele and E.W.N. Glover, *Phys. Rev.* **D46** (1992) 1980; in Ref. [51], Vol. 2, page 163.
- [32] Z. Kunszt and P. Nason, Proceedings of the Workshop ‘*Z Physics at LEP 1*’, ed. by G. Altarelli, R. Kleiss and C. Verzegnassi, CERN Yellow Report No. 89-08, Vol. 1, page 373; in Ref. [51], Vol. 2, page 163.
- [33] S. Catani and M.H. Seymour, in Ref. [51], Vol. 2, page 163.
- [34] Z. Nagy and Z. Trócsányi, *Phys. Rev. Lett.* **79** (1997) 3604; *Phys. Lett.* **B414** (1997) 187; talk presented at the Euroconference on Quantum Chromodynamics: QCD 97: 25th Anniversary of QCD, Montpellier, France, 3-9 July 1997, preprint C97-07-03.1, August 1997, [hep-ph/9708344](#).
- [35] A. Signer, *Comp. Phys. Commun.* **106** (1997) 125.

- [36] J.M. Campbell, M. Cullen and E.W.N. Glover, in preparation.
- [37] S. Catani, G. Turnock, B.R. Webber and L. Trentadue, preprint Cavendish-HEP-90/16, August 1990 (unpublished); *Nucl. Phys.* **B407** (1993) 3;
G. Dissertori and M. Schmelling, *Phys. Lett.* **B361** (1995) 167.
- [38] N. Brown and W.J. Stirling, *Phys. Lett.* **B252** (1990) 657.
- [39] S. Catani, Yu.L. Dokshitzer, M. Olsson, G. Turnock and B.R. Webber, *Phys. Lett.* **B269** (1991) 432.
- [40] N. Brown and W.J. Stirling, *Z. Phys.* **C53** (1992) 629.
- [41] S. Catani, Yu.L. Dokshitzer, F. Fiorani and B.R. Webber, *Nucl. Phys.* **B377** (1992) 445.
- [42] L3 Collaboration, B. Adeva *et al.*, *Phys. Lett.* **B248** (1990) 464;
OPAL Collaboration, M.Z. Akrawy *et al.*, *Phys. Lett.* **B235** (1990) 389;
OPAL Collaboration, M.Z. Akrawy *et al.*, *Z. Phys.* **C49** (1991) 375;
ALEPH Collaboration, D. Decamp *et al.*, *Phys. Lett.* **B255** (1991) 623;
DELPHI Collaboration, P. Abreu *et al.*, *Phys. Lett.* **B247** (1990) 167;
DELPHI Collaboration, P. Abreu *et al.*, *Z. Phys.* **C54** (1992) 55;
ALEPH Collaboration, D. Decamp *et al.*, *Phys. Lett.* **B284** (1992) 163;
OPAL Collaboration, P.D. Acton *et al.*, *Z. Phys.* **C55** (1992) 1;
ALEPH Collaboration, D. Buskulic *et al.*, *Z. Phys.* **C55** (1992) 39;
ALEPH Collaboration, D. Buskulic *et al.*, *Z. Phys.* **C55** (1992) 209;
OPAL Collaboration, P.D. Acton *et al.*, *Z. Phys.* **C59** (1993) 1.
- [43] See for a review:
Chapter 12.5 of Ref. [1] (and references therein).
- [44] L3 Collaboration, B. Adeva *et al.*, *Phys. Lett.* **B263** (1991) 551;
DELPHI Collaboration, P. Abreu *et al.*, *Phys. Lett.* **B274** (1992) 498;
OPAL Collaboration, G. Alexander *et al.*, *Z. Phys.* **C52** (1991) 543.
- [45] L3 Collaboration, B. Adeva *et al.*, *Phys. Lett.* **B248** (1990) 227;
OPAL Collaboration, M.Z. Akrawy *et al.*, *Z. Phys.* **C49** (1991) 49.
- [46] DELPHI Collaboration, P. Abreu *et al.*, *Phys. Lett.* **B255** (1991) 466;
ALEPH Collaboration, D. Decamp *et al.*, *Phys. Lett.* **B284** (1992) 151;
DELPHI Collaboration, P. Abreu *et al.*, *Z. Phys.* **C59** (1993) 357;

- L3 Collaboration, B. Adeva *et al.*, *Phys. Lett.* **B248** (1990) 227;
 OPAL Collaboration, R. Akers *et al.*, *Z. Phys.* **C65** (1995) 367;
 K. Hamacher, Proceedings of the XXVIIIth International Conference on High Energy Physics, Warsaw, Poland, 25-31 July 1996, page 749.
- [47] ALEPH Collaboration, R. Barate *et al.*, *Z. Phys.* **C76** (1997) 1.
- [48] L3 Collaboration, B. Adeva *et al.*, *Phys. Lett.* **B248** (1990) 227;
 OPAL Collaboration, M.Z. Akrawy *et al.*, *Z. Phys.* **C49** (1991) 49.
- [49] L. Lönnblad and T. Sjöstrand, *Phys. Lett.* **B351** (1995) 293.
- [50] G. Gustafson, U. Pettersson and P.M. Zerwas, *Phys. Lett.* **B209** (1988) 90;
 T. Sjöstrand and V.A. Khoze, *Phys. Rev. Lett.* **72** (1994) 28; *Z. Phys.* **C62** (1994) 281;
 G. Gustafson and J. Häkkinen, *Z. Phys.* **C64** (1994) 659.
- [51] Proceedings of the Workshop ‘Physics at LEP2’, eds. G. Altarelli, T. Sjöstrand and F. Zwirner, CERN Report 96-01.
- [52] Proceedings of the ‘LEP2 Phenomenology Workshop’, Oxford, UK, 14-18 April 1997, *J. Phys.* **G24** (1998) 271.
- [53] See, e.g.:
 Proceedings of the Workshop ‘ e^+e^- Collisions at 500 GeV. The Physics Potential’, Munich, Annecy, Hamburg, ed. P.M. Zerwas, DESY 92-123 A/B/C, 1992-1993;
 Proceedings of the Workshop ‘Physics with e^+e^- Colliders’, Annecy, Gran Sasso, Hamburg, ed. P.M. Zerwas, DESY 97-100, May 1997.
- [54] T. Ohl, Proceedings of CRAD’96, Third International Symposium on Radiative Corrections, Cracow, 1-5 August 1996, *Acta Phys. Pol.* **B28** (1997) 847.
- [55] E. Accomando, A. Ballestrero and M. Pizzio, *Nucl. Phys.* **B512** (1998) 19.
- [56] F. Yuasa and Y. Kurihara, in preparation.
- [57] G. Montagna, M. Moretti, O. Nicrosini and F. Piccinini, *Eur. Phys. J.* **C2** (1998) 483.
- [58] E. Accomando, A. Ballestrero and E. Maina, *Phys. Lett.* **B362** (1995) 141.
- [59] F.A. Berends, W.L. van Neerven and G.J. Burgers, *Nucl. Phys.* **B297** (1988) 429;
 Erratum, *ibidem* **B304** (1988) 95;
 E.A. Kuraev and V.S. Fadin, *Sov. J. Nucl. Phys.* **41** (1985) 466;
 G. Altarelli and G. Martinelli, Proceedings of the Workshop ‘Physics at LEP’, eds. J.

- Ellis and R. Peccei, Gèneva, 1986, CERN 86-02;
R. Kleiss, *Nucl. Phys.* **B347** (1990) 29;
O. Nicrosini and L. Trentadue, *Phys. Lett.* **B196** (1987) 551; *Z. Phys.* **C39** (1988) 479.
- [60] G. Montagna, O. Nicrosini and F. Piccinini, *Phys. Lett.* **B406** (1997) 243.
- [61] See, e.g.:
C. Itzykson and J.-B. Zuber, “Quantum Field Theory” (McGraw-Hill, 1985).
- [62] M. Jacob and J.C. Wick, *Ann. Phys.* **7** (1959) 404.
- [63] J.D. Bjorken and M.C. Chen, *Phys. Rev.* **D154** (1966) 1335;
O. Reading-Henry, *Phys. Rev.* **154** (1967) 1534.
- [64] P. De Causmaecker, R. Gastmans, W. Troosts and T. T. Wu, *Phys. Lett.* **B105** (1981) 215; *Nucl. Phys.* **B206** (1982) 53;
F.A. Berends, R. Kleiss, P. de Causmaecker, R. Gastmans, W. Troosts and T. T. Wu, *Nucl. Phys.* **B206** (1982) 61; *ibidem* **B239** (1984) 382; *ibidem* **B239** (1984) 395; *ibidem* **B264** (1986) 243; *ibidem* **B264** (1986) 265.
- [65] M. Caffo and E. Remiddi, *Helv. Phys. Acta.* **55** (1982) 339.
- [66] G.R. Farrar and F. Neri, *Phys. Lett.* **B130** (1983) 109.
- [67] G. Passarino, *Phys. Rev.* **D28** (1983) 2867; *Nucl. Phys.* **B237** (1984) 249.
- [68] F.A. Berends, P.H. Daverveldt and R. Kleiss *Nucl. Phys.* **B253** (1985) 441.
- [69] R. Kleiss and W.J. Stirling, *Nucl. Phys.* **B262** (1985) 235.
- [70] R. Kleiss and W.J. Stirling, *Phys. Lett.* **B179** (1986) 159.
- [71] J. Gunion and Z. Kunszt, *Phys. Lett.* **B161** (1985) 333.
- [72] K. Hagiwara and D. Zeppenfeld, *Nucl. Phys.* **B274** (1986) 1.
- [73] C. Mana and M. Martinez, *Nucl. Phys.* **B287** (1987) 601.
- [74] A. Ballestrero and E. Maina, *Phys. Lett.* **B350** (1995) 225.
- [75] Z. Xu, Da-Hua Zhang and L. Chang, *Nucl. Phys.* **B291** (1987) 392.
- [76] H. Murayama, I. Watanabe and K. Hagiwara, HELAS: HELicity Amplitude Subroutines for Feynman Diagram Evaluations, *KEK Report* 91-11, January 1992.

- [77] S. Moretti, *Phys. Rev.* **D50** (1994) 2016.
- [78] D. Zeppenfeld, *Int. J. Mod. Phys.* **A3** (1980) 2175.
- [79] P. Cvitanovic, *Phys. Rev.* **D14** (1976) 1536.
- [80] G.P. Lepage, *Jour. Comp. Phys.* **27** (1978) 192.
- [81] JADE Collaboration, W. Bartel *et al.*, *Phys. Lett.* **B123** (1983) 460; *Z. Phys.* **33** (1986) 23.
- [82] Yu.L. Dokshitzer, contribution cited in Report of the Hard QCD Working Group, Proc. Workshop on Jet Studies at LEP and HERA, Durham, December 1990, *J. Phys.* **G17** (1991) 1537.
- [83] Yu.L. Dokshitzer, G.D. Leder, S. Moretti and B.R. Webber, *J. High En. Phys.* **8** (1997) 1.
- [84] G.D. Leder, *Nucl. Phys.* **B497** (1997) 334.
- [85] S. Bethke, Z. Kunszt, D.E. Soper and W.J. Stirling, *Nucl. Phys.* **B370** (1992) 310.
- [86] A. Signer and L. Dixon, *Phys. Rev. Lett.* **78** (1997) 811.
- [87] For a review, see, e.g.;
S. Bethke, in Proceedings of the 42nd Scottish Universities Summer School in Physics on ‘High Energy Phenomenology’, August 1-21 1993, St. Andrews, UK.
- [88] T. Sjöstrand, *Comp. Phys. Commun.* **39** (1984) 347;
M. Bengtsson and T. Sjöstrand, *Comp. Phys. Commun.* **43** (1987) 367.
- [89] G. Marchesini, B.R. Webber, G. Abbiendi, I.G. Knowles, M.H. Seymour and L. Stanco, *Comp. Phys. Commun.* **67** (1992) 465.
- [90] T. Sjöstrand, *Comp. Phys. Commun.* **82** (1994) 74.
- [91] R. Odorico, *Comp. Phys. Commun.* **59** (1990) 527.
- [92] L. Lönnblad, *Comp. Phys. Commun.* **71** (1992) 15.
- [93] G. Cowan, in Ref. [52].
- [94] S. Moretti and W.J. Stirling, preprint RAL-TR-1998-037, DTP/98/32, Cavendish-HEP-97/12, July 1998.

- [95] J. André and T. Sjöstrand, *Phys. Rev.* **D57** (1998) 5767;
J. André, preprint LU-TP-97-12, June 1997, hep-ph/9706325.
- [96] G. Marchesini, B.R. Webber, I.G. Knowles, M.H. Seymour, G. Corcella, S. Moretti and K. Odagiri, in preparation.
- [97] E. Fahri, *Phys. Rev. Lett.* **39** (1977) 1587.
- [98] Mark-J Collaboration, D.P. Barber *et al.*, *Phys. Rev. Lett.* **43** (1979) 830.
- [99] G. Parisi, *Phys. Lett.* **B74** (1978) 65;
J.F. Donoghue, F.E. Low and S.Y. Pi, *Phys. Rev.* **D20** (1979) 2759.
- [100] T. Chandrahoman and L. Clavelli, *Nucl. Phys.* **B184** (1981) 365.
- [101] J.D. Bjorken and S.J. Brodsky, *Phys. Rev.* **D1** (1970) 1416.
- [102] S. Catani and B.R. Webber, *J. High En. Phys.* **10** (1997) 5; *Phys. Lett.* **B427** (1998) 377.
- [103] For a review, see [93] and references therein.
- [104] ALEPH Collaboration, ‘QCD studies with e^+e^- annihilation data at 130, 136, 161 and 172 GeV’, contribution to EPS-HEP97, Jerusalem, 19-26 August 1997, reference number 629.
- [105] G. Gustafson, U. Pettersson and P.M. Zerwas, *Phys. Lett.* **B209** (1988) 90;
T. Sjöstrand and V.A. Khoze, *Phys. Rev. Lett* **72** (1994) 28; *Z. Phys.* **C62** (1994) 281;
G. Gustafson and J. Häkkinen, *Z. Phys.* **C64** (1994) 659;
L. Lönnblad, *Z. Phys.* **C70** (1996) 107;
J. Ellis and K. Geiger, *Phys. Lett.* **B404** (1997) 230.
- [106] B. Andersson, G. Gustafson, G. Ingelman and T. Sjöstrand, *Phys. Rep.* **97** (1983) 31.
- [107] T. Sjöstrand and V.A. Khoze, in Ref. [105].
- [108] ‘Determination of the Mass of the W Boson’, Z. Kunszt *et al.*, in ‘Physics at LEP2’, eds. G. Altarelli, T. Sjöstrand and F. Zwirner, CERN Report 96-01, Vol.1, p.141-205 (1996).
- [109] See, e.g.:
B.R. Webber, in Ref. [52].

- [110] P. Igo-Kemenes (convener) and J.H. Kühn (advisor), in Ref. [53], part A, page 255.
- [111] P. Igo-Kemenes (convener) and J.H. Kühn (advisor), in Ref. [53], part A, page 327.
- [112] T.L. Barklow, P. Bussey, P. Chen, M. Drees, R.M. Godbole, W. Kozanecki, F. Richard and J.C. Sens, in Ref. [53], part B, page 837.
- [113] T. Barklow, P. Chen and W. Kozanecki, in Ref. [53], part B, page 845.
- [114] O. Nicrosini and L. Trentadue, in Ref. [59].
- [115] See, e.g.:
 Proceedings of the Workshop on Photon Radiation from Quarks, S. Cartwright ed.,
 Annecy, France, 2-3 Dec. 1991. CERN 92-04;
 OPAL Collaboration, G. Alexander *et al.*, *Phys. Lett.* **B264** (1991) 219;
 OPAL Collaboration, P.D. Acton *et al.*, *Z. Phys.* **C 54** (1992) 193;
 ALEPH Collaboration, D. Decamp *et al.*, *Phys. Lett.* **B264** (1991) 476;
 DELPHI Collaboration, P. Abreu *et al.*, *Z. Phys.* **C 53** (1992) 555;
 L3 Collaboration, O. Adriani *et al.*, *Phys. Lett.* **B292** (1992) 472.
- [116] E.W.N. Glover and A.G. Morgan, *Z. Phys.* **C62** (1994) 311;
 A. Gerhmann-De Ridder and E.W.N. Glover, *Nucl. Phys.* **B517** (1998) 269.
- [117] J. Häkkinen and H. Kharraziha, *Comput. Phys. Commun.* **100** (1997) 311.

6 Appendix I

In this Appendix we present the analytical expressions for the helicity amplitudes relevant to the three processes (1)–(3). As already mentioned, we make use of the formalism introduced through Refs. [69, 73, 74, 77]. Each amplitude will be expressed in terms of a suitable combination of the X and Z functions defined in Subsect. 2.1 (and of scalar products involving the external four-momenta). The directions of the latter are such that the both the initial state electrons and positrons and all the partons $q, q', q'', \bar{q}, \bar{q}', \bar{q}'' g$ in the final states are considered outgoing.

In order to minimise the lenght of the formulae, we adopt the following short-hand notations. The index (a) (i.e., in round brackets) stands for the momentum p_a and the corresponding polarization λ_a of any real particle $a = 1, \dots, 8$. In the case where external gluons are involved, additional indices will appear, such as $[a]$ (i.e., in squared brackets), to which are associated the auxiliary momentum q_a of the gluon a and its helicity λ_a (see eq. (16)). The notation $\{k\}$ (i.e., in curly brackets) refers to both the momentum p_k and the internal helicity λ associated to a propagator. We further make the convention that all indices $\{k\}$ are summed over, and that the sum extends to all possible values of all internal helicities, $\lambda, \lambda', \dots = \pm$, as well as to the momenta appearing in the last lines of the forthcoming expressions for the amplitudes of processes (1)–(3) (in the spirit of eq. (5))¹⁶.

To each of the basic amplitudes are associated propagators functions. In the case of off-shell fermions, they have the form

$$D_f(\{i\}) = \frac{1}{(\sum_i p_i)^2 - m_f^2}, \quad (30)$$

whereas in the case of bosons one gets

$$D_V(\{i\}) = \frac{1}{(\sum_i p_i)^2 - M_V^2 + iM_V\Gamma_V}. \quad (31)$$

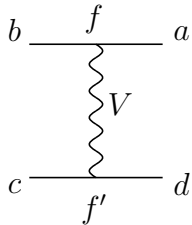
In eqs. (30)–(31), f is the flavour q, q' or q'' of a virtual fermion line, whereas $V = \gamma, Z$ or g , being $M_V = \Gamma_V \equiv 0$ if $V = \gamma$ or g . In order to assign the correct fermionic propagator functions to the various amplitudes, one will have to multiply the latter for as many terms of the form (30) as the number of indices $\{i\}, \dots$ appearing in the last line of the amplitude equations, with the sums \sum_i extending to all the values assumed by i . A subscript of the form $\{\dots\}_f$ will indicate the flavour $f = q, q', q''$ to be assigned to the off-shell fermion line. As for the bosonic propagators in the case $V = g$ (i.e., for gluons), these will only appear in the functions A, B or C (see below). Their appropriate expressions will be given while defining the latter. Finally, as the incoming $V = \gamma, Z$ currents are a common feature to all

¹⁶Note the order of the indices in the sequence $\{a, b, c, \dots\}$ has no importance.

diagrams, we will factorise them in the expressions of the amplitudes, an operation which will be recalled by the use of the subscript V . Given these simple rules, we believe it trivial to derive the correct expressions for all propagators, so these will not appear explicitly in our formulae for the amplitudes. In the latter, we will present the expressions for the topologies of Fig. 3, in the form $T_V^i(\Pi, \{\lambda\})$, with $i = 1, \dots, 8$ for process (1), $i = 1, \dots, 10$ for process (2), and $i = 1, \dots, 3$ for process (3), and where Π represents (a product of) permutations π of gluon colour indices and $\{\lambda\}$ refers to the helicities of the external particles.

As for the couplings, the notation fV refers to the pair of chiral indices (c_R, c_L) entering in the expressions given in Tabs. 1–2 and associated with the vertex involving a fermion $f = e, q, q', q''$ and a gauge vector $V = \gamma, Z, g$, according to Tab. 4. In particular, the notation qg is meant to describe both a true and a fictitious quark-gluon vertex, the latter being used to define the polarization of the gauge particle (for which $(c_R, c_L) \equiv (1, 1)$), according to eq. (16).

Graphically, a Z function is represented as (hereafter, one symbolically has that $\langle \rangle = ()$, $[]$ or $\{\}$)

$$Z(\langle a \rangle; \langle b \rangle; \langle c \rangle; \langle d \rangle; fV; f'V) =$$

(32)

On the same footing as was done in Ref. [30], we found it convenient to introduce the function describing a three-gluon vertex, here generalised to the case of off-shell gauge vectors, each connected to a fermion line¹⁷,

¹⁷Here and in the following, we write the momentum of the gluon attached to the fermion line labelled by ab in terms of those of the others involved. This convention will be helpful both in writing the Feynman diagrams in a more compact analytic form as well as in calculating them numerically in a more efficient manner, as this way the labels a and b only appear as arguments of the A , B and C functions, and not in the internal momentum summations. In fact, the line ab will eventually be identified with the off-shell one connected to the incoming γ, Z current in Fig. 3a–c.

$$\begin{aligned}
A(\langle a \rangle; \langle b \rangle; \langle c \rangle; \langle d \rangle; \langle e \rangle; \langle f \rangle) &= \text{Diagram} \\
&= Z(\langle a \rangle; \langle b \rangle; \langle c \rangle; \langle d \rangle; qg; qg) \\
&\quad \times 2X(\langle e \rangle; \{i\}; \langle f \rangle; qg) \\
&- Z(\langle c \rangle; \langle d \rangle; \langle e \rangle; \langle f \rangle; qg; qg) \\
&\quad \times X(\langle a \rangle; \{i\}; \langle b \rangle; qg) \\
&- \text{same}[(c, d) \leftrightarrow (e, f)]. \tag{33}
\end{aligned}$$

To each A term is always associated the propagator $D_g(\{i\} + \{j\}) \equiv 1/(\sum_i p_i + \sum_j p_j)^2$. Note that the summation $\{i\}$ extends to $i = c, d$ if $\langle d \rangle \neq [d]$, or to $i = c$ otherwise and similarly for $\{j\}$ with respect to the indices e, f . In addition, if $\langle d \rangle \neq [d](\langle f \rangle \neq [f])$, the additional term $D_g(\{i\})(D_g(\{j\}))$ appears.

In addition to eq. (33), we also need the expression describing two connected three-gluon vertices and the associated four-gluon vertex with same colour structure. Assuming again that the gluon propagator connected to ab is expressed in terms of the momenta associated to the legs c, \dots, h , one has

$$B(\langle a \rangle; \langle b \rangle; \langle c \rangle; \langle d \rangle; \langle e \rangle; \langle f \rangle; \langle g \rangle; \langle h \rangle) =$$

$$=$$

$$+$$

$$\begin{aligned}
&= Z(\langle a \rangle; \langle b \rangle; \langle c \rangle; \langle d \rangle; qg; qg) \\
&\times [2(X(\langle g \rangle; \{i\}; \langle h \rangle; qg) + X(\langle g \rangle; \{j\}; \langle h \rangle; qg)) \times \\
&\quad 2X(\langle e \rangle; \{i\}; \langle f \rangle; qg)] \\
&+ Z(\langle a \rangle; \langle b \rangle; \langle g \rangle; \langle h \rangle; qg; qg) Z(\langle c \rangle; \langle d \rangle; \langle e \rangle; \langle f \rangle; qg; qg) \times \\
&\quad (2 \sum_k p_k + \sum_i p_i + \sum_j p_j) \cdot (\sum_i p_i) \\
&+ Z(\langle a \rangle; \langle b \rangle; \langle e \rangle; \langle f \rangle; qg; qg) Z(\langle c \rangle; \langle d \rangle; \langle g \rangle; \langle h \rangle; qg; qg) \times \\
&\quad (\sum_i p_i + \sum_j p_j)^2 \\
&- Z(\langle c \rangle; \langle d \rangle; \langle e \rangle; \langle f \rangle; qg; qg) \\
&\times [2(X(\langle g \rangle; \{i\}; \langle h \rangle; qg) + X(\langle g \rangle; \{j\}; \langle h \rangle; qg))X(\langle a \rangle; \{i\}; \langle b \rangle; qg) + \\
&\quad (X(\langle a \rangle; \{k\}; \langle b \rangle; qg) - X(\langle a \rangle; \{j\}; \langle b \rangle; qg) - X(\langle a \rangle; \{i\}; \langle b \rangle; qg))X(\langle g \rangle; \{i\}; \langle h \rangle; qg)] \\
&+ 2X(\langle e \rangle; \{i\}; \langle f \rangle; qg) \\
&\times [-Z(\langle a \rangle; \langle b \rangle; \langle g \rangle; \langle h \rangle; qg; qg) \\
&\quad \times (2X(\langle c \rangle; \{k\}; \langle d \rangle; qg) + X(\langle c \rangle; \{j\}; \langle d \rangle; qg)) \\
&\quad + Z(\langle c \rangle; \langle d \rangle; \langle g \rangle; \langle h \rangle; qg; qg) \\
&\quad \times (X(\langle a \rangle; \{k\}; \langle b \rangle; qg) - X(\langle a \rangle; \{j\}; \langle b \rangle; qg) - X(\langle a \rangle; \{i\}; \langle b \rangle; qg))] \\
&- \text{same}[(c, d) \leftrightarrow (e, f)]
\end{aligned} \tag{34}$$

The propagators associated to B functions assume the form $D_g(\{i\} + \{j\} + \{k\})D_g(\{i\} +$

$\{j\}) \equiv 1/(\sum_i p_i + \sum_j p_j + \sum_k p_k)^2/(\sum_i p_i + \sum_j p_j)^2$. The summations $\{i\}$, $\{j\}$ and $\{k\}$ are over the indices c, d, e, f and g, h if $\langle d \rangle \neq [d]$, $\langle f \rangle \neq [f]$ and $\langle h \rangle \neq [h]$, or c, e and g otherwise, respectively. Moreover, as previously explained, if $\langle d \rangle \neq [d](\langle f \rangle \neq [f])(\langle h \rangle \neq [h])$, the additional term $D_g(\{i\})(D_g(\{j\}))[D_g(\{k\})]$ has to be inserted.

Finally, we further need the function describing three connected three-gluon vertices and the two associated graphs with one four-gluon and one three-gluon vertex with identical colour matrices,

$$C(\langle a \rangle; \langle b \rangle; \langle c \rangle; \langle d \rangle; \langle e \rangle; \langle f \rangle; \langle g \rangle; \langle h \rangle; \langle i \rangle; \langle j \rangle) =$$

The image displays three Feynman diagrams representing the function C . Each diagram consists of a central three-gluon vertex (represented by a curly line) connected to three three-gluon vertices. The top-left three-gluon vertex has external lines labeled c , d , and e . The top-right three-gluon vertex has external lines labeled b , a , and j . The bottom three-gluon vertex has external lines labeled i , g , and h . The diagrams are separated by plus signs, indicating they are summed together.

$$\begin{aligned}
&= \{ (2X(\langle i \rangle; \{k\}; \langle j \rangle; qg) + 2X(\langle i \rangle; \{l\}; \langle j \rangle; qg) + 2X(\langle i \rangle; \{m\}; \langle j \rangle; qg) + X(\langle i \rangle; \{n\}; \langle j \rangle; qg)) \\
&\quad \times [2(X(\langle g \rangle; \{k\}; \langle h \rangle; qg) + X(\langle g \rangle; \{l\}; \langle h \rangle; qg)) \times \\
&\quad (2X(\langle e \rangle; \{k\}; \langle f \rangle; qg) Z(\langle a \rangle; \langle b \rangle; \langle c \rangle; \langle d \rangle; qg; qg) - \\
&\quad X(\langle a \rangle; \{k\}; \langle b \rangle; qg) Z(\langle c \rangle; \langle d \rangle; \langle e \rangle; \langle f \rangle; qg; qg)) \\
&\quad + (X(\langle a \rangle; \{m\}; \langle b \rangle; qg) - X(\langle a \rangle; \{l\}; \langle b \rangle; qg) - X(\langle a \rangle; \{k\}; \langle b \rangle; qg)) \times \\
&\quad (2X(\langle e \rangle; \{k\}; \langle f \rangle; qg) Z(\langle c \rangle; \langle d \rangle; \langle g \rangle; \langle h \rangle; qg; qg) - \\
&\quad X(\langle g \rangle; \{k\}; \langle h \rangle; qg) Z(\langle c \rangle; \langle d \rangle; \langle e \rangle; \langle f \rangle; qg; qg)) \\
&\quad - (2X(\langle c \rangle; \{m\}; \langle d \rangle; qg) + X(\langle c \rangle; \{l\}; \langle d \rangle; qg)) \times \\
&\quad 2X(\langle e \rangle; \{k\}; \langle f \rangle; qg) Z(\langle a \rangle; \langle b \rangle; \langle g \rangle; \langle h \rangle; qg; qg) \\
&\quad + (2 \sum_m p_m + \sum_l p_l + \sum_k p_k) \cdot (\sum_k p_k) \times \\
&\quad Z(\langle a \rangle; \langle b \rangle; \langle g \rangle; \langle h \rangle; qg; qg) Z(\langle c \rangle; \langle d \rangle; \langle e \rangle; \langle f \rangle; qg; qg)] \\
&- \text{same}[(a, b) \leftrightarrow (i, j); \{k\} + \{l\} + \{m\} + \{n\} \leftrightarrow -\{n\}] \\
&+ Z(\langle a \rangle; \langle b \rangle; \langle i \rangle; \langle j \rangle; qg; qg) Z(\langle c \rangle; \langle d \rangle; \langle e \rangle; \langle f \rangle; qg; qg) \\
&\quad \times [2(X(\langle g \rangle; \{k\}; \langle h \rangle; qg) + X(\langle g \rangle; \{l\}; \langle h \rangle; qg)) \times \\
&\quad (\sum_k p_k + \sum_l p_l + \sum_m p_m + 2 \sum_n p_n) \cdot (\sum_k p_k) \\
&\quad + X(\langle g \rangle; \{k\}; \langle h \rangle; qg) \times \\
&\quad (\sum_k p_k + \sum_l p_l + \sum_m p_m + 2 \sum_n p_n) \cdot (\sum_m p_m - \sum_l p_l - \sum_k p_k) \\
&\quad - (X(\langle g \rangle; \{k\}; \langle h \rangle; qg) + X(\langle g \rangle; \{l\}; \langle h \rangle; qg) + 2X(\langle g \rangle; \{n\}; \langle h \rangle; qg)) \times \\
&\quad (\sum_k p_k + \sum_l p_l + 2 \sum_m p_m) \cdot (\sum_k p_k)] \\
&+ 2 Z(\langle a \rangle; \langle b \rangle; \langle i \rangle; \langle j \rangle; qg; qg) X(\langle e \rangle; \{k\}; \langle f \rangle; qg) \\
&\quad \times [Z(\langle c \rangle; \langle d \rangle; \langle g \rangle; \langle h \rangle; qg; qg) \\
&\quad (\sum_k p_k + \sum_l p_l + \sum_m p_m + 2 \sum_n p_n) \cdot (\sum_k p_k + \sum_l p_l - \sum_m p_m) + \\
&\quad (2X(\langle c \rangle; \{m\}; \langle d \rangle; qg) + X(\langle c \rangle; \{l\}; \langle d \rangle; qg)) \times \\
&\quad (X(\langle g \rangle; \{k\}; \langle h \rangle; qg) + X(\langle g \rangle; \{l\}; \langle h \rangle; qg) + 2X(\langle g \rangle; \{n\}; \langle h \rangle; qg)) - \\
&\quad 2(2X(\langle c \rangle; \{n\}; \langle d \rangle; qg) + X(\langle c \rangle; \{m\}; \langle d \rangle; qg) + X(\langle c \rangle; \{l\}; \langle d \rangle; qg))] \times \\
&\quad (X(\langle g \rangle; \{k\}; \langle h \rangle; qg) + X(\langle g \rangle; \{l\}; \langle h \rangle; qg))] \\
&+ (\sum_k p_k + \sum_l p_l + \sum_m p_m)^2 \times \\
&\quad \{Z(\langle a \rangle; \langle b \rangle; \langle g \rangle; \langle h \rangle; qg; qg) \times \\
&\quad [2Z(\langle c \rangle; \langle d \rangle; \langle i \rangle; \langle j \rangle; qg; qg) X(\langle e \rangle; \{k\}; \langle f \rangle; qg) -
\end{aligned}$$

$$\begin{aligned}
& Z(\langle c \rangle; \langle d \rangle; \langle e \rangle; \langle f \rangle; qg; qg) X(\langle i \rangle; \{k\}; \langle j \rangle; qg) \\
& - Z(\langle g \rangle; \langle h \rangle; \langle i \rangle; \langle j \rangle; qg; qg) \times \\
& [2Z(\langle a \rangle; \langle b \rangle; \langle c \rangle; \langle d \rangle; qg; qg) X(\langle e \rangle; \{k\}; \langle f \rangle; qg) - \\
& Z(\langle c \rangle; \langle d \rangle; \langle e \rangle; \langle f \rangle; qg; qg) X(\langle a \rangle; \{k\}; \langle b \rangle; qg)] \} \\
& + (\sum_k p_k + \sum_l p_l)^2 Z(\langle c \rangle; \langle d \rangle; \langle g \rangle; \langle h \rangle; qg; qg) \times \\
& [2Z(\langle a \rangle; \langle b \rangle; \langle e \rangle; \langle f \rangle; qg; qg) \times \\
& (X(\langle i \rangle; \{k\}; \langle j \rangle; qg) + X(\langle i \rangle; \{l\}; \langle j \rangle; qg) + X(\langle i \rangle; \{m\}; \langle j \rangle; qg)) + \\
& Z(\langle e \rangle; \langle f \rangle; \langle i \rangle; \langle j \rangle; qg; qg) \times \\
& (X(\langle a \rangle; \{n\}; \langle b \rangle; qg) - X(\langle a \rangle; \{m\}; \langle b \rangle; qg) - \\
& X(\langle a \rangle; \{l\}; \langle b \rangle; qg) - X(\langle a \rangle; \{k\}; \langle b \rangle; qg)) - \\
& Z(\langle a \rangle; \langle b \rangle; \langle i \rangle; \langle j \rangle; qg; qg) \times \\
& (2X(\langle e \rangle; \{n\}; \langle f \rangle; qg) + X(\langle e \rangle; \{m\}; \langle f \rangle; qg) + X(\langle e \rangle; \{l\}; \langle f \rangle; qg))] \\
& - \text{same}[(c, d) \leftrightarrow (e, f)]. \tag{35}
\end{aligned}$$

The propagator functions associated to these terms are of the form $D_g(\{k\} + \{l\} + \{m\} + \{n\})D_g(\{k\} + \{l\} + \{m\})D_g(\{k\} + \{l\}) \equiv 1/(\sum_k p_k + \sum_l p_l + \sum_m p_m + \sum_n p_n)^2/(\sum_k p_k + \sum_l p_l + \sum_m p_m)^2/(\sum_k p_k + \sum_l p_l)^2$. The summations $\{k\}$, $\{l\}$, $\{m\}$ and $\{n\}$ are here over c, d, e, f, g, h and i, j if $\langle d \rangle \neq [d]$, $\langle f \rangle \neq [f]$, $\langle h \rangle \neq [h]$ and $\langle j \rangle \neq [j]$, or c, e, g and i otherwise, in the same order. Also in this case, terms of the forms $D_g(\{k\})$, $D_g(\{l\})$, $D_g(\{m\})$ and $D_g(\{n\})$ will appear if $\langle d \rangle \neq [d]$, $\langle f \rangle \neq [f]$, $\langle h \rangle \neq [h]$ and/or $\langle j \rangle \neq [j]$, respectively.

Note that further manipulations would be possible, though in the form given in eqs. (33), (34) and (35), the functions A , B and C are suitable for immediate implementation in a numerical program, as we have done in our calculations. The expressions (32), (33), (34) and (35) are now the basic ingredients needed to describe the spinor part of all the topologies appearing in Fig. 3a–c.

In the remainder of this Appendix, we present the helicity amplitudes associated to the typical topologies in Fig. 3a–c, stripped off their colour structure (operation that we recall by means of the introduction of the argument Π). For sake of illustration, we assume that the labels a and b always refer to the quarks and antiquarks of flavour q in all reactions (1)–(3), that c and d refer to gluons in reaction (1) and to the quarks and antiquarks of flavour q' in reactions (2)–(3) and that e and f refer to gluons in reactions (1)–(2) and to the quarks and antiquarks of flavour q'' in reaction (3). The permutations chosen as example for the gluons labelled $cdef$ in reaction (1) and ef in reaction (2) as well those for the internal coloured gauge vectors in processes (2)–(3) ought to be self-evident in the forthcoming helicity amplitudes.

$$e^+(p_1, \lambda_1) + e^-(p_2, \lambda_2) \rightarrow q(p_a, \lambda_a) + \bar{q}(p_b, \lambda_b) + g(p_c, \lambda_c) + g(p_d, \lambda_d) + g(p_e, \lambda_e) + g(p_f, \lambda_f)$$

$$\begin{aligned}
T_1^V(\Pi, \{\lambda\}) &= Z((a); \{i\}; (c); [c]; qg; qg) \\
&\times Z(\{i\}; \{j\}; (d); [d]; qg; qg) \\
&\times Z(\{j\}; \{k\}; (1); (2); qV; eV) \\
&\times Z(\{k\}; \{l\}; (e); [e]; qg; qg) \\
&\times Z(\{l\}; (b); (f); [f]; qg; qg), \\
&\{i\} = \{a, c\}_q, \quad \{j\} = \{a, c, d\}_q, \quad \{k\} = \{1, 2, a, c, d\}_q, \\
&\{l\} = \{1, 2, a, c, d, e\}_q.
\end{aligned} \tag{36}$$

$$\begin{aligned}
T_2^V(\Pi, \{\lambda\}) &= A((a); \{i\}; (c); [c]; (d); [d]) \\
&\times Z(\{i\}; \{j\}; (1); (2); qV; eV) \\
&\times Z(\{j\}; \{k\}; (e); [e]; qg; qg) \\
&\times Z(\{k\}; (b); (f); [f]; qg; qg), \\
&\{i\} = \{a, c, d\}_q, \quad \{j\} = \{1, 2, a, c, d\}_q, \quad \{k\} = \{1, 2, a, c, d, e\}_q.
\end{aligned} \tag{37}$$

$$\begin{aligned}
T_3^V(\Pi, \{\lambda\}) + T_4^V(\Pi, \{\lambda\}) &= B((a); \{i\}; (c); [c]; (d); [d]; (e); [e]) \\
&\times Z(\{i\}; \{j\}; (1); (2); qV; eV) \\
&\times Z(\{j\}; (b); (f); [f]; qg; qg), \\
&\{i\} = \{a, c, d, e\}_q, \quad \{j\} = \{1, 2, a, c, d, e\}_q.
\end{aligned} \tag{38}$$

$$\begin{aligned}
T_5^V(\Pi, \{\lambda\}) &= A((a); \{i\}; (c); [c]; (d); [d]) \\
&\times Z(\{i\}; \{j\}; (1); (2); qV; eV) \\
&\times A(\{j\}; (b); (e); [e]; (f); [f]), \\
&\{i\} = \{a, c, d\}_q, \quad \{j\} = \{1, 2, a, c, d\}_q.
\end{aligned} \tag{39}$$

$$\begin{aligned}
T_6^V(\Pi, \{\lambda\}) + T_7^V(\Pi, \{\lambda\}) + T_8^V(\Pi, \{\lambda\}) &= T((a); \{i\}; (1); (2); qV; eV) \\
&\times C(\{i\}; (b); (c); [c]; (d); [d]; (e); [e]; (f); [f]), \\
&\{i\} = \{1, 2, a\}_q.
\end{aligned} \tag{40}$$

$$e^+(p_1, \lambda_1) + e^-(p_2, \lambda_2) \rightarrow q(p_a, \lambda_a) + \bar{q}(p_b, \lambda_b) + q'(p_c, \lambda_c) + \bar{q}'(p_d, \lambda_d) + g(p_e, \lambda_e) + g(p_f, \lambda_f)$$

$$\begin{aligned}
T_1^V(\Pi, \{\lambda\}) &= Z((a); \{i\}; (c); (d); qg; qg) \\
&\times Z(\{i\}; \{j\}; (1); (2); qV; eV) \\
&\times A(\{j\}; (b); (e); [e]; (f); [f]), \\
\{i\} &= \{a, c, d\}_q, \quad \{j\} = \{1, 2, a, c, d\}_q.
\end{aligned} \tag{41}$$

$$\begin{aligned}
T_2^V(\Pi, \{\lambda\}) &= Z((a); \{i\}; (c); (d); qg; qg) \\
&\times Z(\{i\}; \{j\}; (1); (2); qV; eV) \\
&\times Z(\{j\}; \{k\}; (e); [e]; qg; qg) \\
&\times Z(\{k\}; (b); (f); [f]; qg; qg), \\
\{i\} &= \{a, c, d\}_q, \quad \{j\} = \{1, 2, a, c, d\}_q, \quad \{k\} = \{1, 2, a, c, d, e\}_q.
\end{aligned} \tag{42}$$

$$\begin{aligned}
T_3^V(\Pi, \{\lambda\}) &= Z((a); \{i\}; \{k\}; (d); qg; qg) \\
&\times Z((c); \{k\}; (e); [e]; qg; qg) \\
&\times Z(\{i\}; \{j\}; (1); (2); qV; eV) \\
&\times Z(\{j\}; (b); (f); [f]; qg; qg), \\
\{i\} &= \{a, c, d, e\}_q, \quad \{j\} = \{1, 2, a, c, d, e\}_q, \quad \{k\} = \{c, e\}_{q'}.
\end{aligned} \tag{43}$$

$$\begin{aligned}
T_4^V(\Pi, \{\lambda\}) &= A((a); \{i\}; (c); (d); (e); [e]) \\
&\times Z(\{i\}; \{j\}; (1); (2); qV; eV) \\
&\times Z(\{j\}; (b); (f); [f]; qg; qg), \\
\{i\} &= \{a, c, d, e\}_q, \quad \{j\} = \{1, 2, a, c, d, e\}_q.
\end{aligned} \tag{44}$$

$$\begin{aligned}
T_5^V(\Pi, \{\lambda\}) &= Z((a); \{i\}; (1); (2); qV; eV) \\
&\times Z(\{i\}; (b); \{k\}; (d); qg; qg) \\
&\times Z((c); \{j\}; (e); [e]; qg; qg) \\
&\times Z(\{j\}; \{k\}; (f); [f]; qg; qg), \\
\{i\} &= \{1, 2, a\}_q, \quad \{j\} = \{c, e\}_{q'}, \quad \{k\} = \{c, e, f\}_{q'}.
\end{aligned} \tag{45}$$

$$\begin{aligned}
T_6^V(\Pi, \{\lambda\}) &= Z((a); \{i\}; (1); (2); qV; eV) \\
&\times Z(\{i\}; (b); \{j\}; (d); qg; qg) \\
&\times A((c); \{j\}; (e); [e]; (f); [f]), \\
&\{i\} = \{1, 2, a\}_q, \quad \{j\} = \{c, e, f\}_{q'}.
\end{aligned} \tag{46}$$

$$\begin{aligned}
T_7^V(\Pi, \{\lambda\}) + T_8^V(\Pi, \{\lambda\}) + T_9^V(\Pi, \{\lambda\}) &= Z((a); \{i\}; (1); (2); qV; eV) \\
&\times B(\{i\}; (b); (c); (d); (e); [e]; (f); [f]), \\
&\{i\} = \{1, 2, a\}_q.
\end{aligned} \tag{47}$$

$$\begin{aligned}
T_{10}^V(\Pi, \{\lambda\}) &= Z((a); \{i\}; (1); (2); qV; eV) \\
&\times A(\{i\}; (b); \{j\}; (d); (f); [f]) \\
&\times Z((c); \{j\}; (e); [e]; qg; qg), \\
&\{i\} = \{1, 2, a\}_q, \quad \{j\} = \{c, e\}_{q'}.
\end{aligned} \tag{48}$$

$e^+(p_1, \lambda_1) + e^-(p_2, \lambda_2) \rightarrow q(p_a, \lambda_a) + \bar{q}(p_b, \lambda_b) + q'(p_c, \lambda_c) + \bar{q}'(p_d, \lambda_d) + q''(p_e, \lambda_e) + \bar{q}''(p_f, \lambda_f)$

$$\begin{aligned}
T_1^V(\Pi, \{\lambda\}) &= Z((a); \{i\}; (1); (2); qV; eV) \\
&\times Z(\{i\}; (b); \{j\}; (d); qg; qg) \\
&\times Z((c); \{j\}; (e); (f); qg; qg), \\
&\{i\} = \{1, 2, a\}_q, \quad \{j\} = \{c, e, f\}_{q'}.
\end{aligned} \tag{49}$$

$$\begin{aligned}
T_2^V(\Pi, \{\lambda\}) &= Z((a); \{i\}; (c); (d); qg; qg) \\
&\times Z(\{i\}; \{j\}; (1); (2); qV; eV) \\
&\times Z(\{j\}; (b); (e); (f); qg; qg), \\
&\{i\} = \{a, c, d\}_q, \quad \{j\} = \{1, 2, a, c, d\}_q.
\end{aligned} \tag{50}$$

$$\begin{aligned}
T_3^V(\Pi, \{\lambda\}) &= Z((a); \{i\}; (1); (2); qV; eV) \\
&\times A(\{i\}; (b); (c); (d); (e); (f)), \\
\{i\} &= \{1, 2, a\}_q.
\end{aligned} \tag{51}$$

7 Appendix II

In this Appendix we describe how we have proceeded to obtain the QCD colour factors¹⁸ relevant to the three reactions (1)–(3). In what follows, we assume that all internal and external colours are always summed over.

The amplitudes squared for processes (1)–(3), summed/averaged over the final/initial colours and spins, can be written in the general form

$$|\overline{M}|^2 = \frac{1}{4} g_s^4 e^2 \left(\prod_i N_i \right) \left(\prod_p \frac{1}{n_p!} \right) \sum_{\{\lambda\}} \sum_{\Pi, \Pi'} M(\Pi, \{\lambda\}) M^*(\Pi', \{\lambda\}) C^{\Pi, \Pi'}. \tag{52}$$

The factor $1/4$ accounts for the average over the initial spins whereas the EM and QCD couplings are obtained via the relations $e = \sqrt{4\pi\alpha_{em}}$ and $g_s = \sqrt{4\pi\alpha_s}$ (in natural units) from the constants introduced in Subsect. 2.3. In the above equation $\Pi^{(\prime)}$ represents (products of) permutations of the gluon indices, $\{\lambda\}$ indicates the helicities of all external particles λ_i (with $i = 1, \dots, 8$), $M(\Pi^{(\prime)}, \{\lambda\})$ is the coefficient of the colour matrix $T_f^{\Pi^{(\prime)}}$ (where f represents a sequence of flavours $ij\dots$), that is, the full spinor amplitude (here, $\{i\} = \{1, 2\}$)

$$M(\Pi^{(\prime)}, \{\lambda\}) = \sum_{\pi(qq'(q''))} \sum_{i=1}^n \left(\sum_{V=\gamma, Z} T_V^i(\Pi^{(\prime)}, \{\lambda\}) D_V(\{i\}) \right), \tag{53}$$

with $n = 8, 10$ and 3 for process (1), (2) and (3), respectively, and $C^{\Pi, \Pi'}$ is the appropriate colour factor, $C^{\Pi, \Pi'} = \text{Tr}(T_f^{\Pi} T_f^{\Pi'\dagger})$. Here, $\sum_{\pi(qq'(q''))}$ refers to the sum over all possible flavour permutations in events with at least four quarks. Furthermore, $n_p!$ is a statistical factor corresponding to each n_p -tuple of identical final state particles p appearing in reactions (1)–(3)¹⁹ whereas N_i is the normalisation of the fermion current associated to the gluon i , see eq. (17). In reaction (1) $p = g$ and $n_g = 4$, for (2) one has $p = q, \bar{q}, g$ with $n_q \equiv n_{\bar{q}} = 1(2)$ if $q \neq q'(q = q')$ and $n_g = 2$, whereas for (3) one gets $p = q, \bar{q}$ with $n_q \equiv n_{\bar{q}} = 1(2)[3]$ if $q \neq q' \neq q''(q = q' \neq q'')[q = q' = q'']$. As for the gluon normalisations, the product \prod_i extends to $i = 5, 6, 7, 8$ in (1), to $i = 7, 8$ in (2) whereas it does not appear for (3).

¹⁸In order to check their correctness we have calculated the traces of the QCD matrices both using an analytical procedure as well as the computer program **COLOUR** [117].

¹⁹Therefore, our multidimensional integrations must cover the whole six-particle phase space.

In order to obtain the colour factors $C^{\Pi, \Pi'}$ we have proceeded as follows. First, we have decomposed a four-gluon vertex into three three-gluon vertices, each with a different colour and kinematic structure in *factorised* form. One such decompositions, though not unique, that we have adopted here, is the one pictured in Fig. 17 (from Ref. [117]). Then, we have repeatedly exploited the equation

$$[t^A, t^B]_{ij} \equiv t_{ik}^A t_{kj}^B - t_{ik}^B t_{kj}^A = if^{ABC} t_{ij}^C, \quad (54)$$

relating the matrices t_{ij}^A (with $A = 1, \dots, 8$ gluon and $i, j = 1, \dots, 3$ quark colours) of the fundamental representation to the structure constants f^{ABC} of the SU(3) gauge group²⁰, in order to rewrite the colour parts of diagrams involving triple and quadruple gluon vertices as a combination of the basic colour structures typical of the ‘abelian graphs’, i.e., those non involving gluon self-couplings. If one does so, than the colour piece of each diagram can be expressed as an appropriate combination of different permutations of products involving t_{ij}^A matrices only²¹.

In case of process (1), all colour structures in Fig. 3a are linear combinations of terms of the form (here, $\Pi = \pi$ and $f = ij$)

$$T_{ij}^\pi(q\bar{q}gggg) = (t^A t^B t^C t^D)_{ij}^{\pi(5678)}, \quad (55)$$

where $A, B, C, D(i, j)$ are the gluon(quark) colour and $\pi(5678)$ is one the possible permutations of the gluon indices $A, \dots, D = 5, \dots, 8$. For four external gluons, one has $4!$ of these, that is 24, twelve of which will be cyclical and twelve anticyclical, so that the number of fundamental colour factors $C^{\pi, \pi'}$ needed to describe the colour content of process (1) is 576 in total. These are given in Tab. 6, for the cyclical π' -permutations only, as the remaining colour factors can be obtained by symmetry.

In case of process (2), the colour structures appearing in Fig. 3b can be rewritten as linear combinations of terms of the four forms (here, $\Pi = \pi(\pi\pi')$ in the first(last) two cases and $f = ijkl$)

$$T_{ijkl}^\pi(q\bar{q}q'\bar{q}'gg) = (t^X t^A t^B)_{ij}^{\pi(X78)} (t^X)_{kl}, \quad (56)$$

$$T_{ijkl}^\pi(q\bar{q}q'\bar{q}'gg) = (t^X)_{ij} (t^X t^A t^B)_{kl}^{\pi(X78)} \quad (57)$$

$$T_{ijkl}^{\pi\pi'}(q\bar{q}q'\bar{q}'gg) = (t^X t^A)_{ij}^{\pi(X7)} (t^X t^B)_{kl}^{\pi'(X8)}, \quad (58)$$

²⁰As a possible representation of the generators t_{ij}^A , we have used the Gell-Mann one.

²¹Recall that if more than one coloured fermion line is present, such a combination is not unique, though the final answer obviously is.

$\text{Tr}[T_{ij}^\pi(q\bar{q}gggg)(T_{ij}^{\pi'}(q\bar{q}gggg))^\dagger]$												
$C^{\pi,\pi'}$	5678	5786	5867	6758	6875	6587	7856	7568	7685	8576	8657	8765
5678	256	4	4	4	-5	4	71/2	4	-5	-5	-5	-14
5786	4	256	4	-5	-14	-5	4	4	-5	4	71/2	-5
5867	4	4	256	71/2	-5	4	-5	-5	-14	4	4	-5
6758	4	-5	71/2	256	4	4	-5	4	4	-14	-5	-5
6875	-5	-14	-5	4	256	4	-5	71/2	4	-5	4	4
6587	4	-5	4	4	4	256	-14	-5	-5	-5	4	71/2
7856	71/2	4	-5	-5	-5	-14	256	4	4	4	-5	4
7568	4	4	-5	4	71/2	-5	4	256	4	-5	-14	-5
7685	-5	-5	-14	4	4	-5	4	4	256	71/2	-5	4
8576	-5	4	4	-14	-5	-5	4	-5	71/2	256	4	4
8657	-5	71/2	4	-5	4	4	-5	-14	-5	4	256	4
8765	-14	-5	-5	-5	4	71/2	4	-5	4	4	4	256
5687	-32	40	-32	-1/2	-1/2	-32	31	-1/2	31	-1/2	40	31
5768	-32	-32	40	40	31	-1/2	-1/2	-32	-1/2	-1/2	31	31
5876	40	-32	-32	31	31	-1/2	40	-1/2	31	-32	-1/2	-1/2
6785	-1/2	31	31	-32	-32	40	-1/2	-1/2	-32	31	-1/2	40
6857	-1/2	31	40	40	-32	-32	31	31	-1/2	-1/2	-32	-1/2
6578	-32	-1/2	-1/2	-32	40	-32	31	40	-1/2	31	-1/2	31
7865	31	-1/2	31	-1/2	40	31	-32	40	-32	-1/2	-1/2	-32
7586	-1/2	-32	-1/2	-1/2	31	31	-32	-32	40	40	31	-1/2
7658	40	-1/2	31	-32	-1/2	-1/2	40	-32	-32	31	31	-1/2
8567	-1/2	-1/2	-32	31	-1/2	40	-1/2	31	31	-32	-32	40
8675	31	31	-1/2	-1/2	-32	-1/2	-1/2	31	40	40	-32	-32
8756	31	40	-1/2	31	-1/2	31	-32	-1/2	-1/2	-32	40	-32

Table 6: The colour factors $C^{\pi,\pi'}$, multiplied by 27, for $e^+e^- \rightarrow q\bar{q}gggg$. Permutations π are along columns, permutations π' are along rows. Only half of the 24 π' -permutations are given (cyclic ones), as the remaining colour factors can be obtained by symmetry: the $(1-12) \times (1-12)$ submatrix is identical to the $(13-24) \times (13-24)$ one (transposed), whereas the $(13-24) \times (1-12)$ submatrix is identical to the $(1-12) \times (13-24)$ one transposed.

$$T_4^{\pi\pi'}{}_{ijkl}(q\bar{q}q'\bar{q}'gg) = (t^X t^B)_{ij}^{\pi(X8)} (t^X t^A)_{kl}^{\pi'(X7)}, \quad (59)$$

where $A, B, X(i, j, k, l)$ are the gluon(quark) colour indices and $\pi^{(\prime)}(X78)$, $\pi^{(\prime)}(X7)$ and $\pi^{(\prime)}(X8)$ are again gluon index permutations. The symbol X refers to any internal gluon $X = 1, \dots, 8$ connecting the two quark-antiquark lines of colour ij and kl (and flavours q and q' , respectively). For two external gluons, one has $3! \times 1!$ permutations of the former two kinds and $2! \times 2!$ of the latter, for a total of 400 basic colour factors $C_{mn}^{\Pi, \Pi'}$, with $m, n = 1, 2, 3, 4$. We present these in Tabs. 7–11, for the combinations $mn = 11, 12, 13, 33$ and 34. The colour factors $C_{22(44)}^{\pi, \pi'(\pi\pi', \pi''\pi''')}$ are identical to the $C_{11(33)}^{\pi, \pi'(\pi\pi', \pi''\pi''')}$ ones and the corresponding tables coincide with those numbered 7 and 10 here, respectively (tacitly assuming that the same gluon permutations are now made along different quark colour lines). Further notice that the colour factors $C_{23}^{\pi, \pi'\pi''}$ can be obtained from Tab. 9 by exchanging 7 with 8 in the π' and π'' permutations, as can easily be understood by comparing the corresponding colour diagrams. Finally, the cases $C_{14}^{\pi, \pi'\pi''}$ are identical to the $C_{23}^{\pi, \pi'\pi''}$ ones whereas the $C_{24}^{\pi, \pi'\pi''}$'s coincide with the $C_{13}^{\pi, \pi'\pi''}$'s, so that the combinations $mn = 14$ and 24 can both be deduced from Tab. 9, after appropriately assigning the quark colours ij and kl to the gluon permutations π, π' and π'' .

Decomposing the colour structure of the Feynman diagrams in Fig. 3b in terms of (56)–(59) is very convenient when dealing with diagrams which only differ in the exchange of the flavours, $q \leftrightarrow q'$. In fact, in this case, in order to obtain the colourless part of new diagrams one flips between themselves both the quark and antiquark labels in the expressions of the amplitudes (41)–(48): i.e., $a \leftrightarrow c$ and $b \leftrightarrow d$ (this way, both the momenta and helicities get interchanged). As for the colour factors, these can easily be obtained from Tabs. 7–11, if one notices that the colour matrices in (57) are identical to those of eq. (56) when one interchanges the (anti)quark colour labels, i.e., $i \leftrightarrow k$ and $j \leftrightarrow l$, and so is the case for those in (59) with respect to eq. (58).

In case of identical flavours in process (2), $q = q'$, one further needs to calculate the diagrams which differ (in the spinor part) from the original ones of the case $q \neq q'$ in the exchange of the four-momentum and helicity of *one* of the, say, quarks with those of the other, $a \leftrightarrow c$. Because of Fermi statistics, a minus sign factorises too. However, (anti)quark colour quantum numbers have to be exchanged as well. This introduces new colour structures, identical to those in eqs. (56)–(59) except for the exchange $i \leftrightarrow k$. Clearly, the colour factors building up the squared amplitude of the new set of graphs are identical to those already given in Tabs. 7–11. In contrast, new ones are needed for the interference terms. These appear in the above tables in round brackets (note their different normalisation).

In case of process (3), we recognise the following three basic colour structures, as the

$\text{Tr}[T_{ijkl}^{\pi}(q\bar{q}q'\bar{q}'gg)(T_{ijkl}^{\pi'}(q\bar{q}q'\bar{q}'gg))^{\dagger}]$						
$C_{11}^{\pi,\pi'}$	X78	78X	8X7	87X	X87	7X8
X78	32(-32)	1/2(-1/2)	1/2(-1/2)	5(-5)	-4(4)	-4(4)
78X	1/2(-1/2)	32(-32)	1/2(-1/2)	-4(4)	5(-5)	-4(4)
8X7	1/2(-1/2)	1/2(-1/2)	32(-32)	-4(4)	-4(4)	5(-5)
87X	5(-5)	-4(4)	-4(4)	32(-32)	1/2(-1/2)	1/2(-1/2)
X87	-4(4)	5(-5)	-4(4)	1/2(-1/2)	32(-32)	1/2(-1/2)
7X8	-4(4)	-4(4)	5(-5)	1/2(-1/2)	1/2(-1/2)	32(-32)

Table 7: The colour factors $C_{11}^{\pi,\pi'}$, multiplied by 9, for $e^+e^- \rightarrow q\bar{q}q'\bar{q}'gg$ ($q \neq q'$). In round brackets are given the additional ones needed in the case of identical flavours $q = q'$ (for which the exchange of indices $i \leftrightarrow k$ is understood in one of the two interfering colour structures), multiplied by 27. Permutations π are along columns, permutations π' are along rows. The first three are cyclical permutations, whereas the latter three are anticyclical. Note the symmetry in the colour factors: the $(1-3) \times (1-3)$ submatrix is identical to the $(4-6) \times (4-6)$ one (transposed), whereas the $(1-3) \times (4-6)$ submatrix is identical to the $(4-6) \times (1-3)$ one (transposed).

fundamental ones to calculate all the colour factors pertinent to the graphs in Fig. 3c (here, $\Pi = \pi$ and $f = ijklmn$):

$$T_{1ijklmn}^{\pi}(q\bar{q}q'\bar{q}'q''\bar{q}'') = (t^X t^Y)_{ij}^{\pi(XY)} (t^X)_{kl} (t^Y)_{mn}, \quad (60)$$

$$T_{2ijklmn}^{\pi}(q\bar{q}q'\bar{q}'q''\bar{q}'') = (t^X)_{ij} (t^X t^Y)_{kl}^{\pi(XY)} (t^Y)_{mn}, \quad (61)$$

$$T_{3ijklmn}^{\pi}(q\bar{q}q'\bar{q}'q''\bar{q}'') = (t^X)_{ij} (t^Y)_{kl} (t^X t^Y)_{mn}^{\pi(XY)}, \quad (62)$$

where $X, Y(i, j, k, l, m, n)$ are the gluon(quark) colour indices and $\pi(XY)$ represents gluon index permutations. The symbols X and Y refers to any combination of internal gluons $X, Y = 1, \dots, 8$ interconnecting the three quark-antiquark lines of colour ij , kl and mn (and flavours q , q' and q'' , respectively). In this case, the calculation of the colour factors is much easier. In fact, it is trivial to see that there are only four fundamental ones, of the form $C_{op}^{\pi,\pi'}$, with $o, p = 1, 2, 3$. Two correspond to the case $o = p$, $4/3$ and $-1/6$, and two to the opposite condition, $o \neq p$, $-1/3$ and $7/6$. These values are obtained depending on the way three coloured fermion loops (of flavour $q \neq q' \neq q''$) are connected to each other via four

$\text{Tr}[T_{ijkl}^{\pi}(q\bar{q}q'\bar{q}'gg)(T_{ijkl}^{\pi'}(q\bar{q}q'\bar{q}'gg))^{\dagger}]$						
$C_{12}^{\pi,\pi'}$	X78	78X	8X7	87X	X87	7X8
X78	-3(31)	57/2(-1/2)	-3(31)	-3(-5)	6(-14)	-3(-5)
78X	-3(31)	-3(31)	57/2(-1/2)	-3(-5)	-3(-5)	6(-14)
8X7	57/2(-1/2)	-3(31)	-3(31)	6(-14)	-3(-5)	-3(-5)
87X	-3(-5)	-3(-5)	6(-14)	-3(31)	-3(31)	57/2(-1/2)
X87	6(-14)	-3(-5)	-3(-5)	57/2(-1/2)	-3(31)	-3(31)
7X8	-3(-5)	6(-14)	-3(-5)	-3(31)	57/2(-1/2)	-3(31)

Table 8: The colour factors $C_{12}^{\pi,\pi'}$, multiplied by 9, for $e^+e^- \rightarrow q\bar{q}q'\bar{q}'gg$ ($q \neq q'$). In round brackets are given the additional ones needed in the case of identical flavours $q = q'$ (for which the exchange of indices $i \leftrightarrow k$ is understood in one of the two interfering colour structures), multiplied by 27. Permutations π are along columns, permutations π' are along rows. The first three are cyclical permutations, whereas the latter three are anticyclical. Note the symmetry in the colour factors: the $(1-3) \times (1-3)$ submatrix is identical to the $(4-6) \times (4-6)$ one transposed, whereas the $(1-3) \times (4-6)$ submatrix is identical to the $(4-6) \times (1-3)$ one transposed.

$\text{Tr}[T_{ijkl}^{\pi}(q\bar{q}q'\bar{q}'gg)(T_{ijkl}^{\pi'\pi''}(q\bar{q}q'\bar{q}'gg))^{\dagger}]$				
$C_{13}^{\pi,\pi'\pi''}$	(X7)(X8)	(X7)(8X)	(7X)(X8)	(7X)(8X)
X78	1(-5)	-7/2(-1/2)	1(31)	-7/2(71/2)
78X	-7/2(71/2)	1(-1/2)	28(31)	-8(-5)
8X7	28(4)	-8(-32)	-7/2(-1/2)	1(4)
87X	-7/2(-1/2)	1(4)	-7/2(-5)	1(40)
X87	-8(40)	28(4)	1(-5)	-7/2(-1/2)
7X8	1(31)	-7/2(-5)	-8(-14)	28(31)

Table 9: The colour factors $C_{13}^{\pi,\pi'\pi''}$, multiplied by 9, for $e^+e^- \rightarrow q\bar{q}q'\bar{q}'gg$ ($q \neq q'$). In round brackets are given the additional ones needed in the case of identical flavours $q = q'$ (for which the exchange of indices $i \leftrightarrow k$ is understood in one of the two interfering colour structures), multiplied by 27. Permutations π are along columns, permutations π' and π'' are along rows.

$\text{Tr}[T_{3ijkl}^{\pi\pi'}(q\bar{q}q'\bar{q}'gg)(T_{3ijkl}^{\pi''\pi'''}(q\bar{q}q'\bar{q}'gg))^{\dagger}]$				
$C_{33}^{\pi\pi',\pi''\pi'''}$	(X7)(X8)	(X7)(8X)	(7X)(X8)	(7X)(8X)
(X7)(X8)	32(-32)	-4(4)	-4(4)	1/2(-1/2)
(X7)(8X)	-4(4)	32(40)	1/2(-1/2)	-4(-5)
(7X)(X8)	-4(4)	1/2(-1/2)	32(40)	-4(-5)
(7X)(8X)	1/2(-1/2)	-4(-5)	-4(-5)	32(31)

Table 10: The colour factors $C_{33}^{\pi\pi',\pi''\pi'''}$, multiplied by 9, for $e^+e^- \rightarrow q\bar{q}q'\bar{q}'gg$ ($q \neq q'$). In round brackets are given the additional ones needed in the case of identical flavours $q = q'$ (for which the exchange of indices $i \leftrightarrow k$ is understood in one of the two interfering colour structures), multiplied by 27. Permutations π and π' are along columns, permutations π'' and π''' are along rows.

$\text{Tr}[T_{3ijkl}^{\pi\pi'}(q\bar{q}q'\bar{q}'gg)(T_{4ijkl}^{\pi''\pi'''}(q\bar{q}q'\bar{q}'gg))^{\dagger}]$				
$C_{34}^{\pi\pi',\pi''\pi'''}$	(X8)(X7)	(X8)(7X)	(8X)(X7)	(8X)(7X)
(X7)(X8)	-3(31)	-3(-5)	-3(-5)	57/2(-1/2)
(X7)(8X)	-3(-5)	-3(-1/2)	6(40)	-3(4)
(7X)(X8)	-3(-5)	6(40)	-3(-1/2)	-3(4)
(7X)(8X)	57/2(-1/2)	-3(4)	-3(4)	-3(-32)

Table 11: The colour factors $C_{34}^{\pi\pi',\pi''\pi'''}$, multiplied by 9, for $e^+e^- \rightarrow q\bar{q}q'\bar{q}'gg$ ($q \neq q'$). In round brackets are given the additional ones needed in the case of identical flavours $q = q'$ (for which the exchange of indices $i \leftrightarrow k$ is understood in one of the two interfering colour structures), multiplied by 27. Permutations π and π' are along columns, permutations π'' and π''' are along rows.

gluons. If $o = p$, one of the loops has four attached vectors and the others have two. When $o \neq p$, two loops have three connections and the remaining one only one. (Note that in case of the colour diagrams of process (3) gluon permutations along quark lines are constrained, as two (and only two) gluon connections from each of the interfering diagrams must always be adjacent in the full colour graph.) Once again, it is rather straightforward to calculate all diagrams, and corresponding colour structures, differing only by flavour exchanges, given the explicit expressions of the formulae (49)–(51) and of the colour matrices in eqs. (60)–(62), in terms of external momenta/helicities and flavours, respectively.

Also in case of process (3), if two or more flavours in the final state are identical, more (spinor and colour) diagrams are needed. For the spinor part, the number of graphs doubles(triples) depending on whether two(three) flavours coincide and the additional ones (with respect to the case of all different flavours) can again be obtained by simple relabelling of the relevant momenta and helicities in the formulae (49)–(51), as previously explained. As for colour diagrams, it can immediately be seen that for the cases $q = q' \neq q''$, $q' = q'' \neq q$ and $q'' = q \neq q'$ one has to compute graphs in which two bubbles are connected by 2, 3 or 4 gluons with 2, 1 and 0 additional gluons coupled to only one of the loops, respectively. In correspondence of the three sets of colour graphs, one gets 3, 2 and 1 independent colour factors: i.e., $(1/18, 5/9, -4/9)$, $(-7/18, 1/9)$ and $(-1/3)$. Finally, in the case $q = q' = q''$, the additional colour factors needed for the calculation of the complete ME for process (3) have already been derived, as they appear among the numbers given in Tab. 6. Indeed, one only needs five of those: i.e., 31, -5 , $-1/2$, $71/2$ and 4 (all to be further divided by 27). Also in case of identical flavours the same restrictions as above on the possible gluon permutations in the colour diagrams squared apply.

To appropriately combine the spinor and colour parts of the amplitudes into the matrix elements of the form (52) for all processes (1)–(3) is a tedious but trivial labour that we leave as an exercise for the reader, as it would only results here in cumbersome expressions carrying no additional information with respect to that already given in the previous formulae and tables. This procedure has been implemented in our **FORTRAN** programs, that we make available to the public upon request.

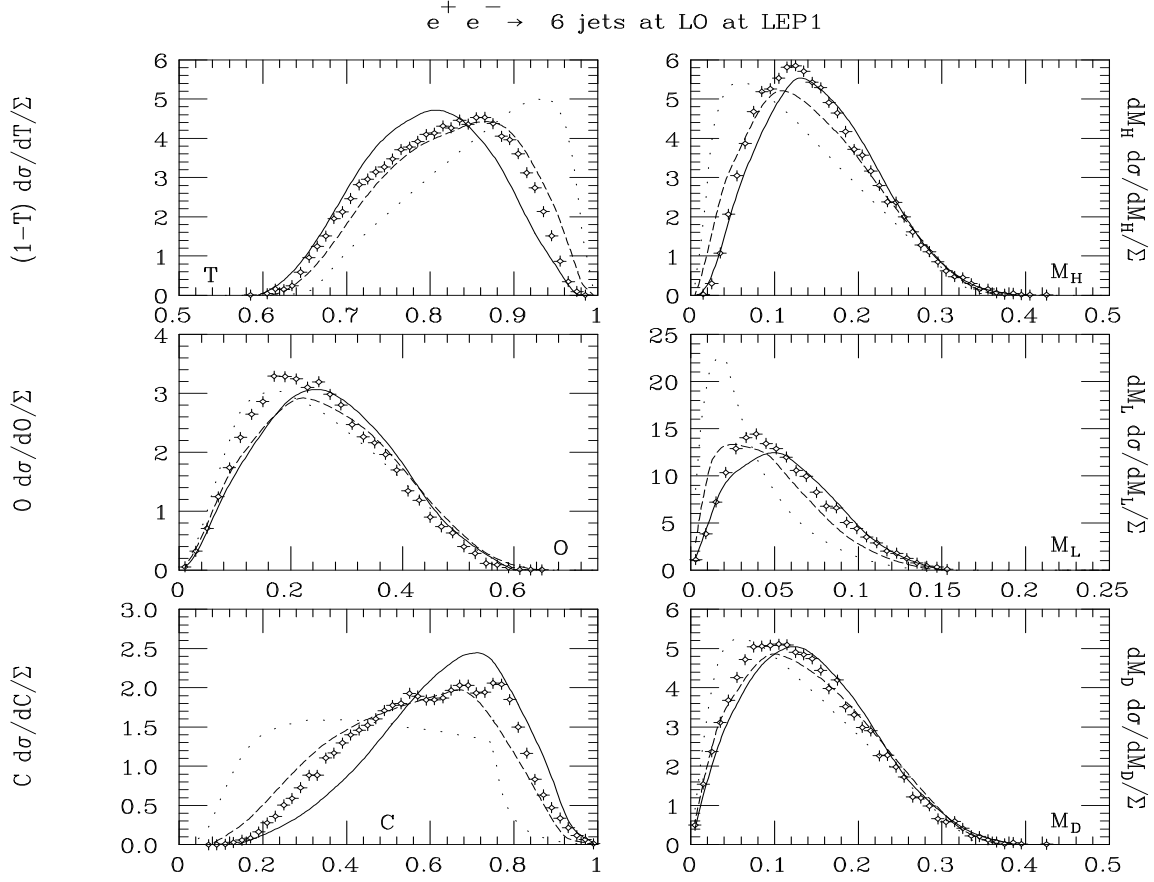


Figure 5: Differential distributions in the following shape variables: thrust (T), oblateness (O), C-parameter (C), heavy (M_H), light (M_L) and difference (M_D) jet mass for the six- (continuous line), five- (dashed line) and four-jet (dotted line) rates at LO, at LEP1. The ‘star’ points correspond instead to the six-jet rate as obtained by using the HERWIG Monte Carlo. The C scheme was used with resolution parameter $y = 0.001$. Notice that the distributions have been normalised to a common factor (one) for readability.

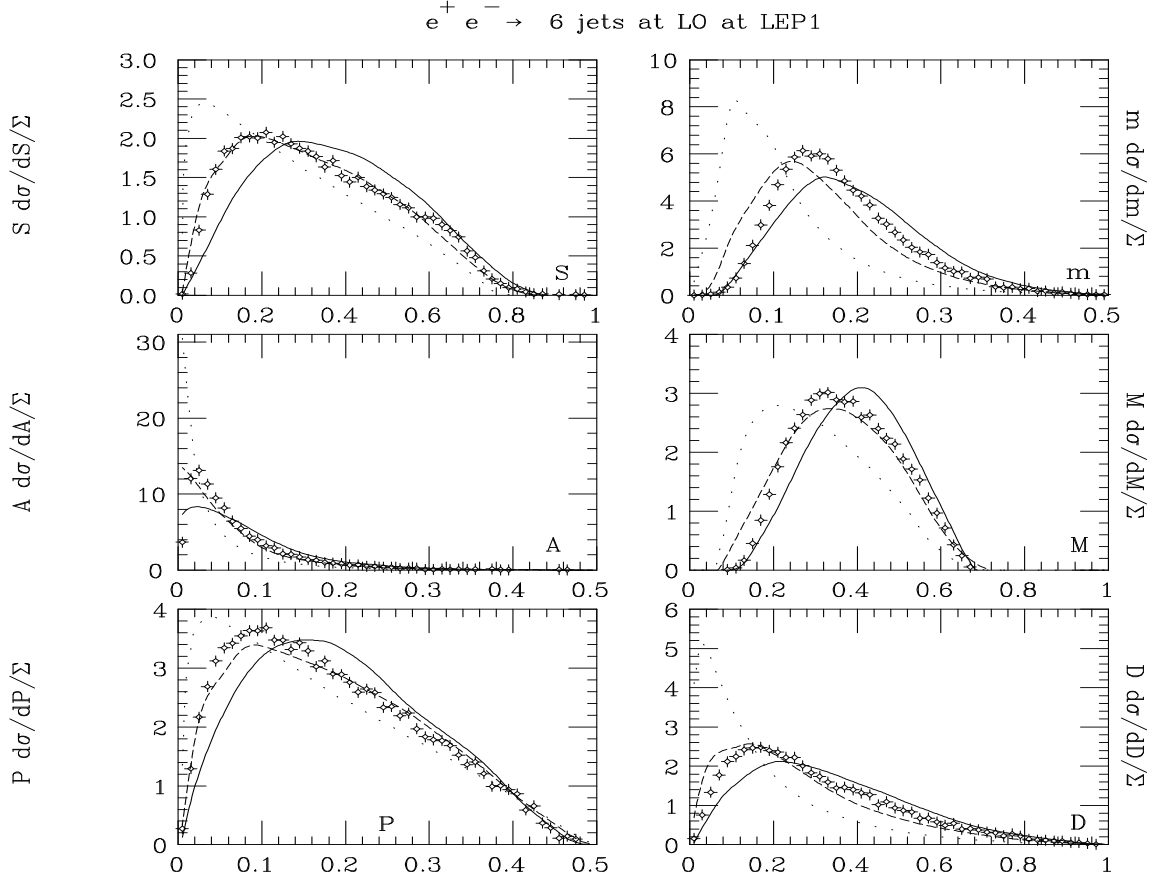


Figure 6: Differential distributions in the following shape variables: sphericity (S), aplanarity (S), planarity (P), minor (m) and major (M) value and D-parameter (D) for the six- (continuous line), five- (dashed line) and four-jet (dotted line) rates at LO, at LEP1. The ‘star’ points correspond instead to the six-jet rate as obtained by using the HERWIG Monte Carlo. The C scheme was used with resolution parameter $y = 0.001$. Notice that the distributions have been normalised to a common factor (one) for readability.

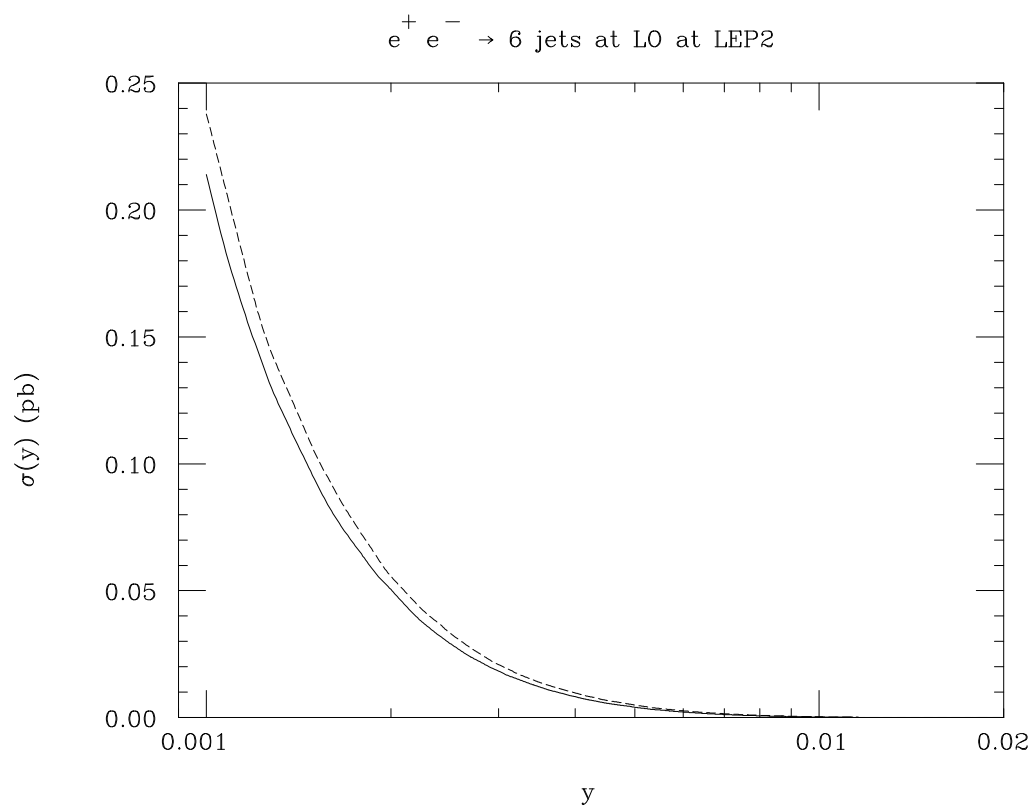


Figure 7: The total cross section of six-jet events at LO in the D (continuous line) and C (dashed line) schemes, at LEP2.

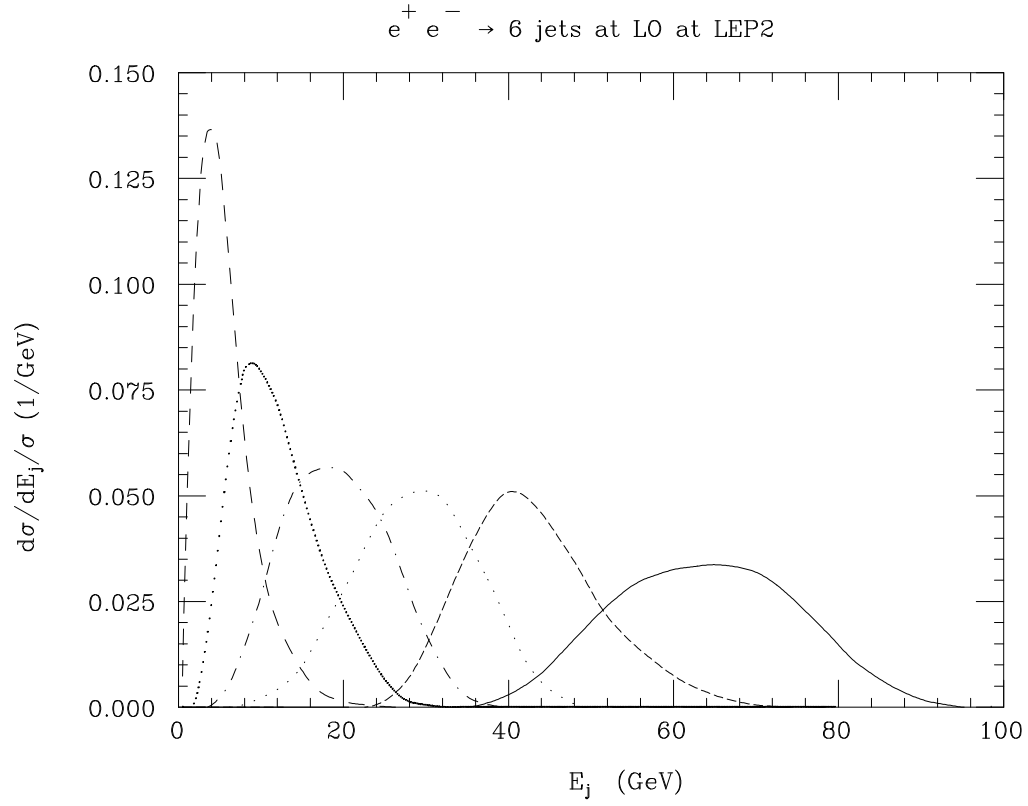


Figure 8: The energy spectra E_j of six-jet events at LO in the J scheme for $y = 0.001$, at LEP2 (here, $\sqrt{s} = 175$ GeV). Jets are energy-ordered such that $E_1 > E_2 > \dots > E_5 > E_6$: $j = 1$ (continuous line), $j = 2$ (short-dashed line), $j = 3$ (dotted line), $j = 4$ (dot-dashed line), $j = 5$ (fine-dotted line) and $j = 6$ (long-dashed line). Normalisation is to unity.

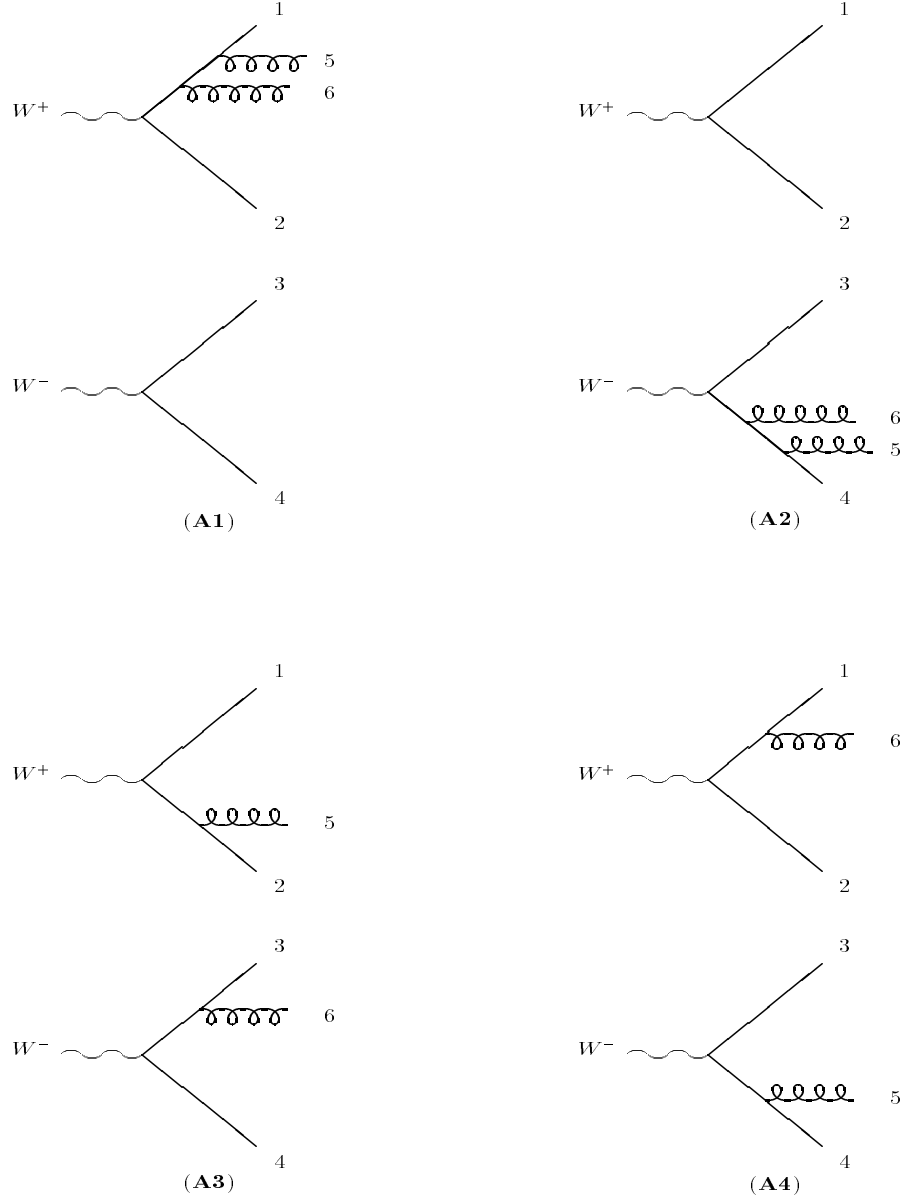


Figure 9: Subsets of Feynman diagrams contributing to $q\bar{q}q'g$ production via W^+W^- . For simplicity the leptonic part of the diagrams is not shown. Permutations are not shown either.

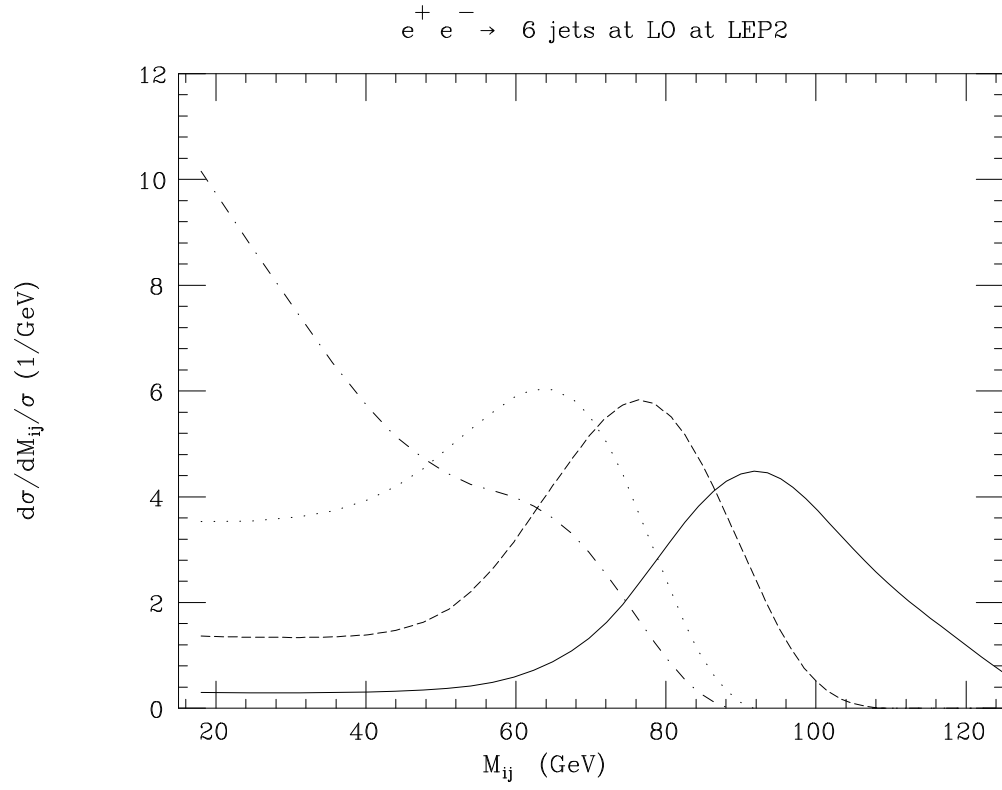


Figure 10: The distributions in the true invariant mass M_{ij} of events of the type (1)–(3) at LO in the C scheme with $y = 0.001$, at LEP2, for the following combinations of parton pairs ij : 12 (continuous lines), 13 (dashed lines), 14 (dotted lines) and 23 (dot-dashed lines).

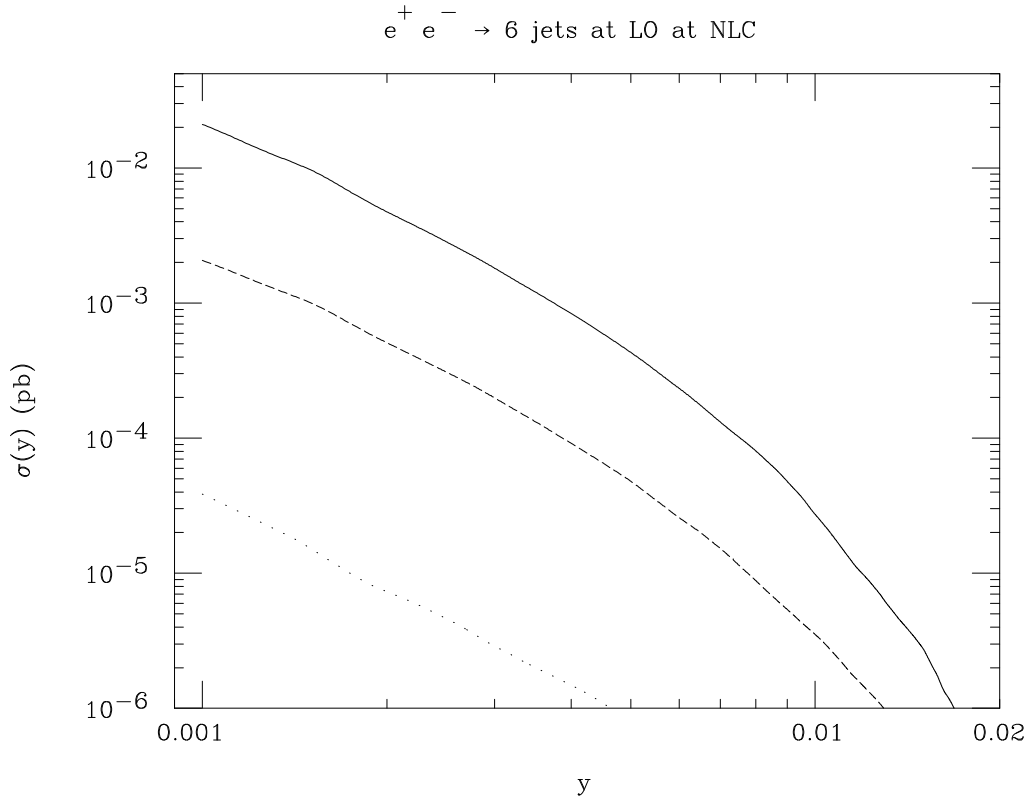


Figure 11: The total cross section of six-jet events at LO in the C scheme, at NLC, decomposed in terms of the three contributions $e^+e^- \rightarrow q\bar{q}gggg$ (continuous line), $e^+e^- \rightarrow q\bar{q}q'\bar{q}'gg$ (dashed line) and $e^+e^- \rightarrow q\bar{q}q'\bar{q}'q''\bar{q}''$ (dotted line).

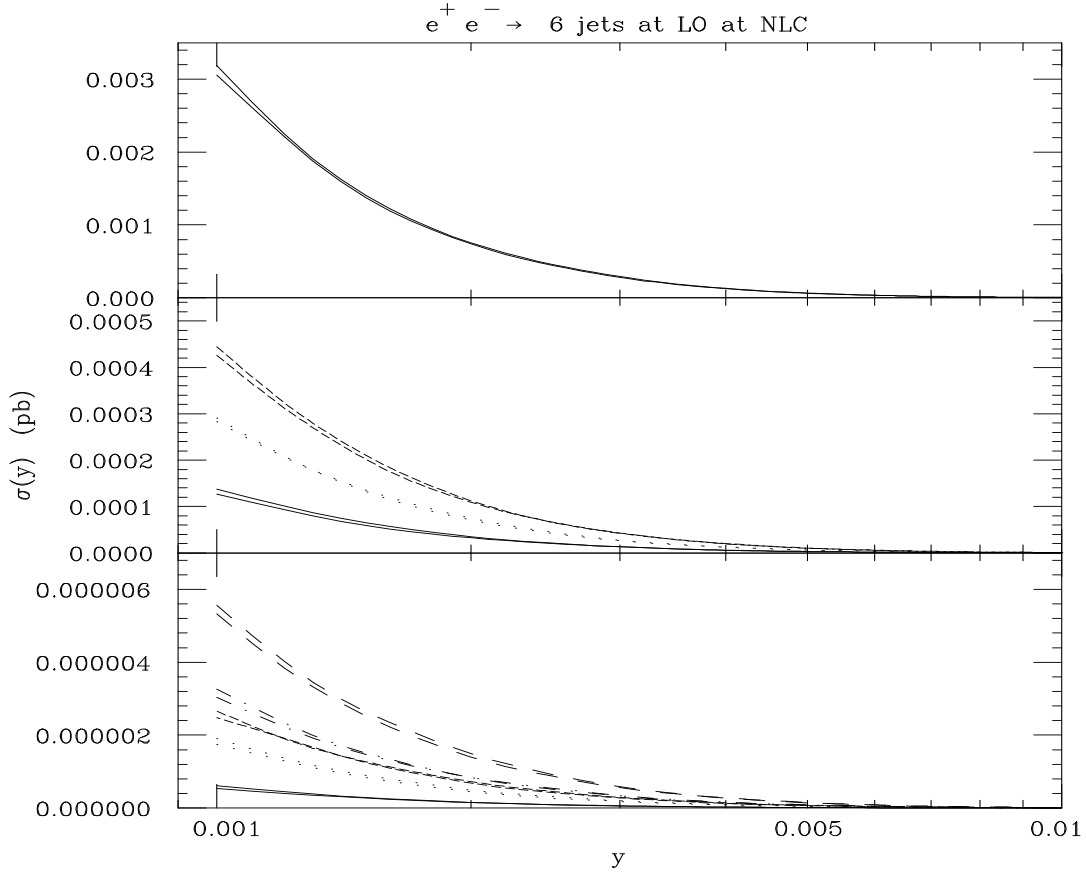


Figure 12: The total cross section of six-jet events at LO in the C scheme, at NLC, decomposed in terms of the contributions containing b -quarks. Upper plot: $e^+e^- \rightarrow b\bar{b}gggg$ (continuous line). Middle plot: $e^+e^- \rightarrow b\bar{b}b\bar{b}gg$ (continuous line), $e^+e^- \rightarrow b\bar{b}u\bar{u}gg$ (dashed line) and $e^+e^- \rightarrow b\bar{b}d\bar{d}gg$ (dotted line). Lower plot: $e^+e^- \rightarrow b\bar{b}b\bar{b}b\bar{b}$ (continuous line), $e^+e^- \rightarrow b\bar{b}b\bar{b}u\bar{u}$ (short-dashed line), $e^+e^- \rightarrow b\bar{b}b\bar{b}d\bar{d}$ (dotted line), $e^+e^- \rightarrow b\bar{b}u\bar{u}u\bar{u}$ (dot-dashed line) and $e^+e^- \rightarrow b\bar{b}u\bar{u}d\bar{d}$ (long-dashed line); here, the case $e^+e^- \rightarrow b\bar{b}d\bar{d}d\bar{d}$ has not been reproduced as it visually coincides with $e^+e^- \rightarrow b\bar{b}b\bar{b}d\bar{d}$. In the upper lines $m_b = 0$, in the lower lines $m_b = 4.25$ GeV.

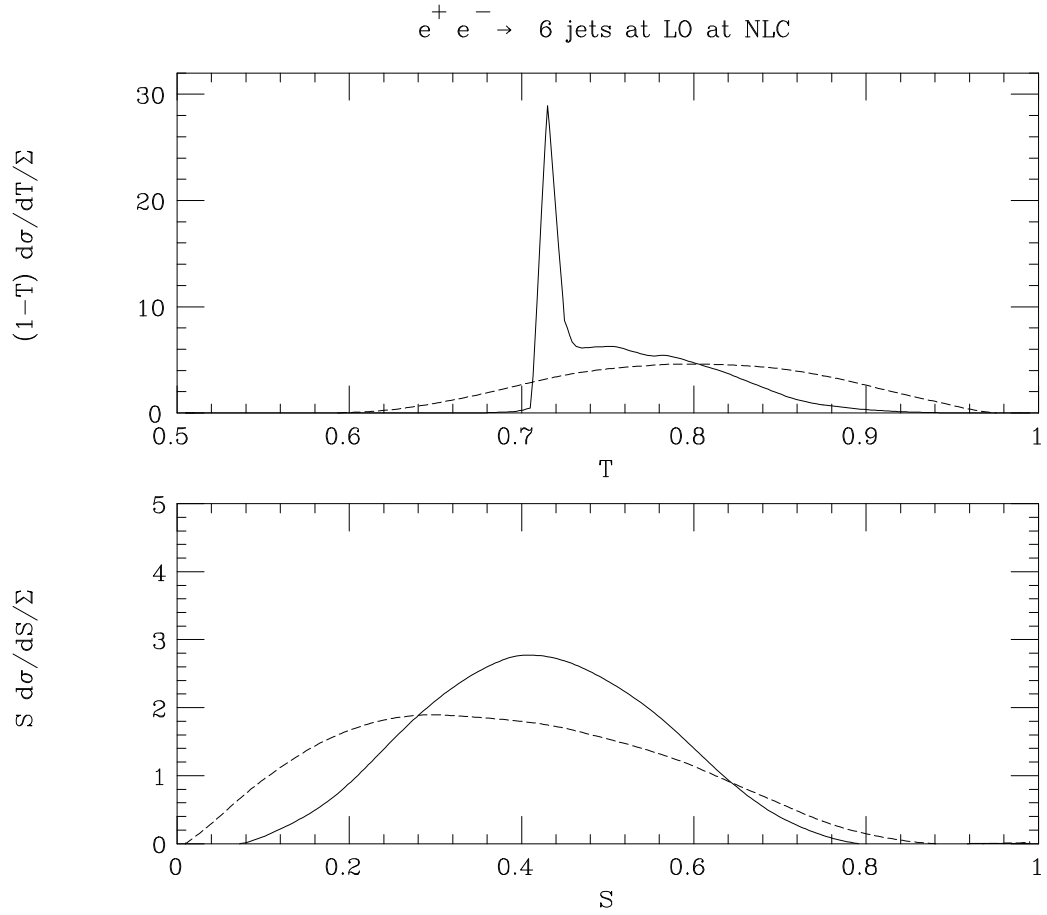


Figure 13: The distributions in thrust (upper plot) and sphericity (lower plot) for $e^+ e^- \rightarrow t\bar{t} \rightarrow 6\text{-jet}$ events (continuous line) and for those of the type (1)–(3) (dashed line) at LO in the C scheme with $y = 0.001$, at NLC. Notice that the distributions have been normalised to a common factor (one) for readability.

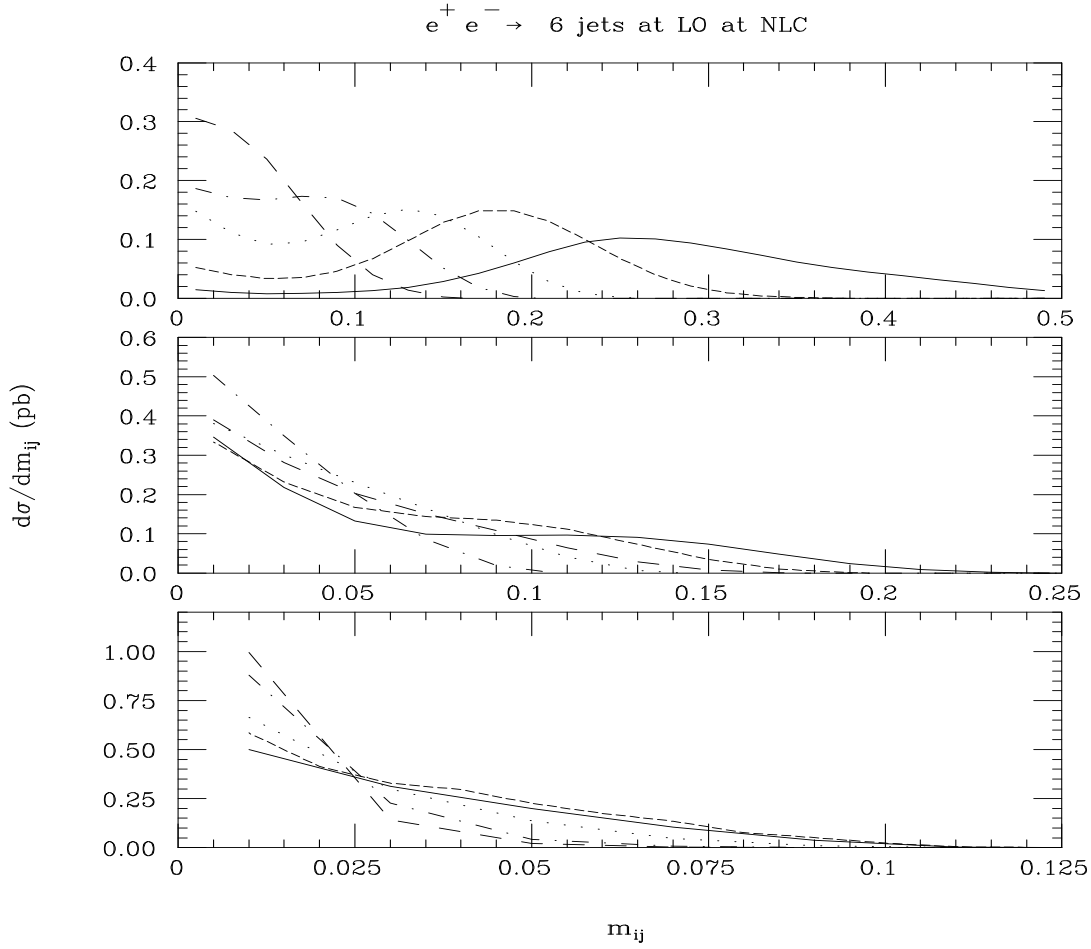


Figure 14: The distributions in the reduced invariant mass m_{ij} (29) for events of the type (1)–(3) at LO in the C scheme with $y = 0.001$, at NLC, for the following combinations of parton pairs ij : (12)[23]{35} (continuous lines), (13)[24]{36} (short-dashed lines), (14)[25]{45} (dotted lines), (15)[26]{46} (dot-dashed lines) and (16)[34]{56} (long-dashed lines), in the (upper)[central]{lower} frame.

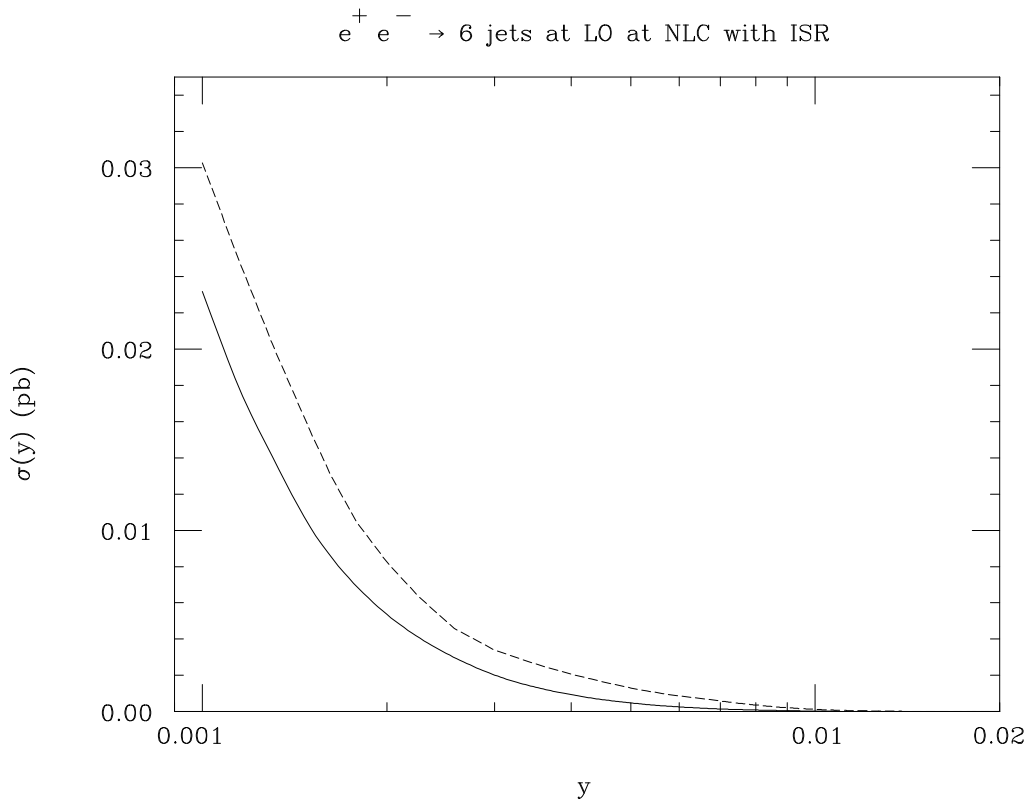


Figure 15: The total cross section of six-jet events at LO in the D scheme, at NLC, without (solid line) and with (dashed line) ISR.

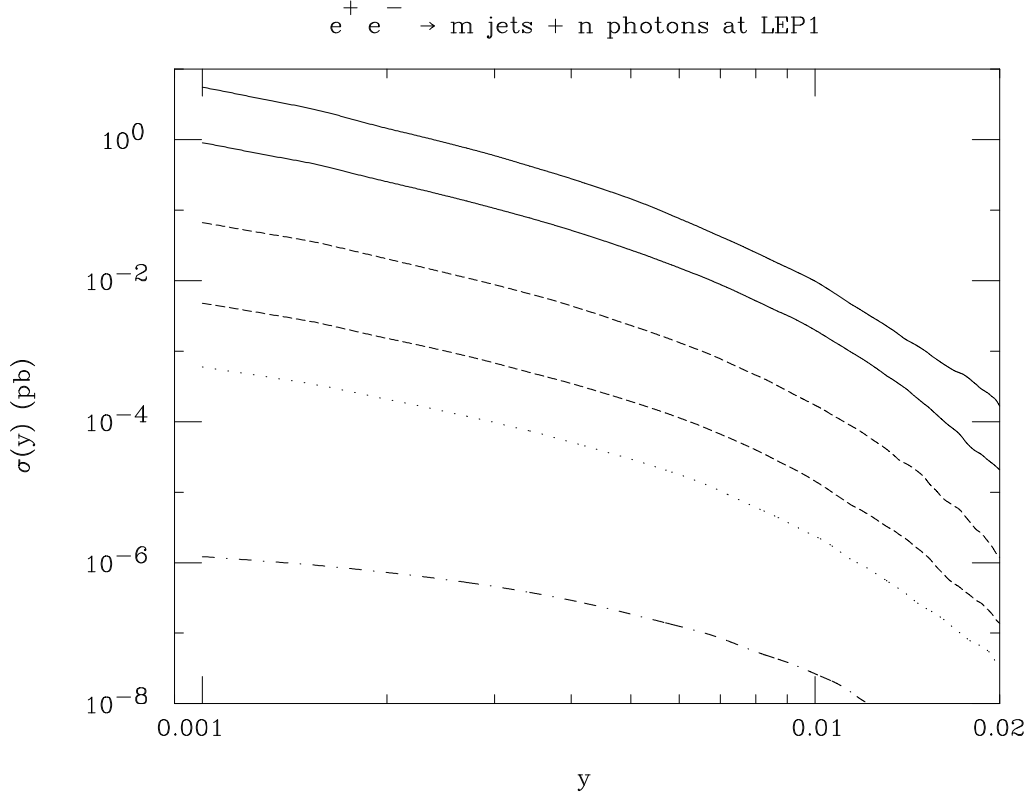


Figure 16: The total cross section for photoproduction at LO in the C scheme, at LEP1, for the processes: $e^+e^- \rightarrow q\bar{q}ggg\gamma$ and $e^+e^- \rightarrow q\bar{q}q'\bar{q}'g\gamma$ ($m=5, n=1$: continuous lines), $e^+e^- \rightarrow q\bar{q}gg\gamma\gamma$ and $e^+e^- \rightarrow q\bar{q}q'\bar{q}'\gamma\gamma$ ($m=4, n=2$: dashed lines), $e^+e^- \rightarrow q\bar{q}g\gamma\gamma\gamma$ ($m=3, n=3$: dotted line) and $e^+e^- \rightarrow q\bar{q}\gamma\gamma\gamma\gamma$ ($m=2, n=4$: dot-dashed line). In the cases $m=5, n=1$ and $m=4, n=2$ the upper lines represent the two-quark contributions whereas the lower ones refer to four-quark processes. The following additional cuts have been introduced on the photons: $p_T^\gamma > 5 \text{ GeV}$ and $|\cos\theta_\gamma| < 0.85$.

$$\begin{aligned}
& \begin{array}{c} \alpha \quad \delta \\ \diagdown \quad \diagup \\ \bullet \\ \diagup \quad \diagdown \\ \beta \quad \gamma \end{array} \Rightarrow \begin{array}{c} \left. \begin{array}{c} \diagup \quad \diagdown \\ \bullet \end{array} \right\} \text{---} \left. \begin{array}{c} \diagdown \quad \diagup \\ \bullet \end{array} \right\} \left[g^{\alpha\gamma} g^{\beta\delta} - g^{\alpha\delta} g^{\beta\gamma} \right] + \\
\begin{array}{c} \diagup \quad \diagdown \\ \bullet \\ \diagdown \quad \diagup \\ \bullet \end{array} \left[g^{\alpha\gamma} g^{\beta\delta} - g^{\alpha\beta} g^{\gamma\delta} \right] + \\
\begin{array}{c} \diagup \quad \diagdown \\ \bullet \\ \diagdown \quad \diagup \\ \bullet \end{array} \left[g^{\alpha\delta} g^{\beta\gamma} - g^{\alpha\beta} g^{\gamma\delta} \right]
\end{array}
\end{aligned}$$

Figure 17: A symbolic representation of the decomposition of a quadruple-gluon vertex into three triple-gluon vertices.